N. M. Patrikalakis
C. Chryssostomidis

Nonlinear Statics of Nonrotationally Uniform Rods With Torsion

MIT Sea Grant
College Program

Massachusetts
Institute of Technology
Cambridge, MA 02139

MITSG 85-18
December 1985

NON-LINEAR STATICS OF NON-ROTATIONALLY UNIFORM RODS WITH TORSION

by

N. M. Patrikalakis

C. Chryssostomidis

MIT Sea Grant Report No. 85-18

September 1985

Sea Grant College Program
Massachusetts Institute of Technology
Cambridge, MA 02139

Grant No.: NA84-AA-D-00046
Project No.: R/T-5

publication date: December 1985

ABSTRACT

The objectives of this work are to:

- Formulate the static problem of a compliant riser idealized as a slender non-rotationally uniform rod with bending, extensional and torsional degrees of freedom.
- Present an embedding technique used to solve the general two-dimensional and three-dimensional static problems of a buoyant compliant riser.
- Present examples from the static analysis of buoyant compliant riser configurations in the presence and absence of external currents.

ACKNOWLEDGEMENTS

Funding for this research was obtained from the MIT Sea Grant College Program, Chevron, Conoco, and Minerals Management Service. G.A. Kriezis assisted in the preparation of figures. M. Chryssostomidis prepared the reference list.

RELATED SEA GRANT REPORTS

1. A Mathematical Model for Compliant Risers, by N. M. Patrikalakis and C. Chryssostomidis, MIT Sea Grant Report No. 85-17, 1985.

2. Linear Dynamics of Compliant Risers, by N. M. Patrikalakis and C. Chryssostomidis, MIT Sea Grant Report No. 85-19, 1985.

NOMENCLATURE

$A_i, A_o; A_b$	total inner and outer cross-sectional area of riser tubes; total outer cross-sectional area of riser tubes and buoyancy modules
B_b	buoyancy per unit length of buoyancy modules in water
B^*	$\rho_w g A_o$ for $y \leq h_w$ and zero otherwise
c	mean internal fluid speed; for our application $\rho_i c^2 << p$
C	centroid of a cross-section
C_o	static rotation matrix
C_D, C_f	normal mean drag and tangential frictional coefficients
C_D'	drag coefficient of a buoyancy module for flow parallel to $\vec{\zeta}_o$
D	maximum dimension of a cross-section
D^ξ, D^η	dimensions of the cross-section of Figure 2-1
E	Young's modulus
EA	extensional rigidity
$EI^{\xi\xi}, EI^{\eta\eta}$	maximum and minimum bending rigidities of a cross-section
$EI_e^{\xi\xi}, EI_e^{\eta\eta}$	effective rigidities $EI^{\xi\xi} - c^2 J_i^{\xi\xi}; EI^{\eta\eta} - c^2 J_i^{\eta\eta}$

$\vec{F}_H$ external hydrodynamic force per unit length (excluding gravity effects):

$$\vec{F}_H = [F_H^{\zeta}, F_H^{\xi}, F_H^{\eta}]. U''$$

g acceleration of gravity

GI^P, GI_e^P torsional and effective torsional rigidity

$$GI^P - c^2 J_i^{\zeta\zeta}$$

h_i, h_w internal fluid and salt water elevations above the axes origin

$J_R; J_i$ mass inertia per unit length tensor of riser material and buoyancy modules

$$J_R = \text{diag}[J_R^{\zeta\zeta}, J_R^{\xi\xi}, J_R^{\eta\eta}] ;$$

and internal fluid

$$J_i = \text{diag}[J_i^{\zeta\zeta}, J_i^{\xi\xi}, J_i^{\eta\eta}] ,$$

where diag[ ] stands for diagonal matrix

L, L_b unstretched riser length, buoyancy module length

m^{ζ}, m $(W_R+W_b)/g$, $(W_R+W_i+W_b)/g$

$\vec{M}_H$ external hydrodynamic moment per unit length

p internal overpressure due to well (i.e. total internal static pressure minus p_i')

p_i' internal pressure due to gravity, $\rho_i g(h_i - y)$

p_0 external pressure due to gravity, $\rho_w g(h_w - y)$

P tension in riser material

$P^{\xi\eta}$, $P_e^{\xi\eta}$ wetted perimeter of a cross-section,

$$P_e^{\xi\eta} = P^{\xi\eta} + C_D' (A_b - A_0)/C_f L_b$$

Q^{ξ}, Q^{η} shear force in the $\vec{\xi}$ and $\vec{\eta}$ direction

s^*, s stretched and unstretched length of the centerline

t time

T effective tension

U array of unit vectors $[\vec{i}, \vec{j}, \vec{k}]^T$

U_0'' array of unit vectors $[\vec{\zeta}_0, \vec{\xi}_0, \vec{\eta}_0]^T$

$\vec{V}$ current velocity

$$\vec{V} = [V_x, 0, V_z].U = [V_0^{\xi}, V_0^{\xi}, V_0^{\eta}].U_0''$$

$\vec{V}_0^{\xi\eta}$ $[0, V_0^{\xi}, V_0^{\eta}].\ U_0''$

w effective weight per unit length,

$$w = W_R + W_i + W_b - B_b - B^*$$

W_a average effective weight per unit length in water

W_b, W_i, W_R buoyancy module material, internal fluid and riser materials weights per unit length

x, y, z coordinates of C in the inertial frame

ρ_i, ρ_w internal fluid and salt water densities

ϕ, θ, ψ Euler angles

$\vec{\Omega}$ vector rate of rotation of $C\vec{\zeta}\vec{\xi}\vec{\eta}$ frame along the rod,

$$\vec{\Omega} = [\Omega^{\zeta}, \Omega^{\xi}, \Omega^{\eta}].U''$$

Chapter 1

INTRODUCTION AND OUTLINE

Compliant risers are assemblages of pipes with very small overall bending rigidity used to convey oil from the ocean floor or a subsurface buoy to a surface platform. A compliant riser is permitted to acquire large static deformations because of its small bending rigidity and readjusts its configuration in response to large slow motions of the supporting platforms, to which it is rigidly connected, without excessive stressing. Compliant risers have been used successfully in protected waters in buoy loading stations for tankers. Extensions of shallow water concepts have been recently proposed by the industry as alternatives to conventional production risers, because they simplify the overall production system.

The purpose of this work is to:

- Formulate the static problem of a compliant riser idealized as a slender non-rotationally uniform rod with bending, extensional and torsional degrees of freedom.
- Present an embedding technique to solve the general two-dimensional and three- dimensional static problems of a buoyant compliant riser.
- Present examples from the static analysis of buoyant compliant riser configurations in the presence and absence of external currents.

This work is organized as follows:

- Chapter 2 provides a complete formulation of the static problem together with a summary of the assumptions necessary for its derivation. This Chapter provides the governing equations and boundary conditions and explicit expressions for the external loads.

- Chapter 3 provides a numerical solution algorithm using an embedding technique.

- Chapter 4 provides numerical results for a buoyant riser configuration with uniformly distributed buoyancy modules, and

- Chapter 5 provides numerical results for a buoyant riser configuration with a single large buoyancy module.

Chapter 2

PROBLEM FORMULATION

2.1 Model Assumptions

A mathematical model for the static behavior of slender elastic rods undergoing large deformations with small strains is given in Love [1] and Landau and Lifshitz [2]. The modification to account for dynamic effects and the presence of a heavy fluid inside and outside the tube modelled as a slender rod can be found in Nordgren [3] and Patrikalakis [4]. Methods for the computation of the motion of elastic rods with equal principal stiffnesses and with torque applied at the ends can be found in Nordgren [5,3] and without torque in Garrett [6].

Patrikalakis and Chryssostomidis [7] extended the mathematical model derived in Nordgren [3] and Patrikalakis [4] to allow the computation of non-linear motions of an assemblage of tubes modelled as a non-rotationally uniform slender elastic rod with space varying torque. Their model also accounts for the effects of a steady internal flow.

In this work, we specialize the model developed in Patrikalakis and Chryssostomidis [7] to allow the computation of static responses. The static equations are derived from

the general dynamic equations by setting the components of the velocity and angular velocity equal to zero and replacing the external loads with their mean values. The mean values of the external loads may, however, strongly depend upon the dynamic response, such as in the case of vortex induced dynamic lift, see Patrikalakis and Chryssostomidis [8,9]. Given that the dynamic response depends upon the static response, (e.g. upon the static tension), statics and dynamics are, in fact, non-linearly coupled. We believe that this coupling may be analyzed with an iterative procedure and we, therefore, consider the static loads as given functions of the static orientation and position of the riser and the external excitation.

Following Patrikalakis and Chryssostomidis [7], we summarize the basic assumptions of our mathematical model for the static problem:

1. The compliant riser is modelled as a single non-rotationally uniform rod rather than as an assemblage of interacting rods or shells. We make this idealization in order to reduce the degrees of freedom and to allow analysis of the global behavior of our system with the currently available information on the structural characteristics of such structures.

2. The materials employed in the construction of different layers of compliant risers are assumed to be homogeneous, isotropic and linearly elastic.

3. Strains are assumed to remain uniformly small although deformations may become large.

4. Shearing deformations are neglected, Rayleigh slender beam theory, see Crandall et al [10].

5. Thermal effects are neglected.

Further theoretical and experimental research might be necessary to quantify the errors implied by the above list of assumptions.

2.2 General Three-Dimensional Governing Equations and Boundary Conditions

The static equations are derived from the general dynamic equations, Patrikalakis and Chryssostomidis [7], by setting the components of velocity and angular velocity equal to zero and replacing the external loads with their mean values. This procedure leads to:

1. Three force equations:

$$T_{os}-Q_o^{\xi}\Omega_o^{\eta}+Q_o^{\eta}\Omega_o^{\xi}-Wc_{12}^{o}+F_{Ho}^{\zeta}=0 \tag{2.1}$$

$$Q_{os}^{\xi}-Q_o^{\eta}\Omega_o^{\zeta}+T_o\Omega_o^{\eta}-Wc_{22}^{o}+F_{Ho}^{\xi}=0 \tag{2.2}$$

$$Q_{os}^{\eta}-T_o\Omega_o^{\xi}+Q_o^{\xi}\Omega_o^{\zeta}-Wc_{32}^{o}+F_{Ho}^{\eta}=0 \tag{2.3}$$

2. Three moment equations:

$$(GI_e^{p}\Omega_o^{\xi})_s+(EI_e^{\eta\eta}-EI_e^{\xi\xi})\Omega_o^{\eta}\Omega_o^{\xi}+M_{Ho}^{\zeta}=0 \tag{2.4}$$

$$(EI_e^{\xi\xi}\Omega_o^{\xi})_s+(GI_e^{p}-EI_e^{\eta\eta})\Omega_o^{\zeta}\Omega_o^{\eta}-Q_o^{\eta}=0 \tag{2.5}$$

$$(EI_e^{\eta\eta}\Omega_o^{\eta})_s-(GI_e^{p}-EI_e^{\xi\xi})\Omega_o^{\xi}\Omega_o^{\zeta}+Q_o^{\xi}=0 \tag{2.6}$$

3. Three equations relating the derivatives of the Euler angles with the Euler angles and the components of $\vec{\Omega}$:

$$\phi_{os} = (\Omega_o^{\xi}\sin\psi_o + \Omega_o^{\eta}\cos\psi_o)/\cos\theta_o \tag{2.7}$$

$$\theta_{os} = \Omega_o^{\xi}\cos\psi_o - \Omega_o^{\eta}\sin\psi_o \tag{2.8}$$

$$\psi_{os} = \Omega_o^{\zeta}+\phi_{os}\sin\theta_o \tag{2.9a}$$

or using equation (2.7)

$$\psi_{os} = \Omega_o^{\zeta}+\tan\theta_o(\Omega_o^{\xi}\sin\psi_o+\Omega_o^{\eta}\cos\psi_o) \tag{2.9b}$$

4. Three equations relating the derivatives of the Cartesian coordinates x_o, y_o and z_o with the Euler angles:

$$x_{os} = (1+e_o)\cos\theta_o\cos\phi_o \tag{2.10}$$

$$y_{os} = (1+e_o)\cos\theta_o\sin\phi_o \tag{2.11}$$

$$z_{os} = -(1+e_o)\sin\theta_o \tag{2.12}$$

5. The equation for the stretched arc length s_o^* :

$$s^*_{os} = 1+e_o \tag{2.13}$$

where subscript or superscript o denotes static quantities and subscript s denotes derivative with respect to the unstretched arc length, s, of the centerline. To simplify the notation, subscript o has been omitted in the superscripts ζ , ξ and η .

The elements, c^o_{ij} , of the complete 3 x 3 static rotation matrix, C_o , between U and U_o'' defined by

$$U'_0 = C_0 U \tag{2.14.0}$$

are given below in terms of the static Euler angles:

$$c^o_{11} = \cos\theta_o \cos\phi_o \tag{2.14.1}$$

$$c^o_{12} = \cos\theta_o \sin\phi_o \tag{2.14.2}$$

$$c^o_{13} = -\sin\theta_o \tag{2.14.3}$$

$$c^o_{21} = \sin\theta_o \sin\psi_o \cos\phi_o - \cos\psi_o \sin\phi_o \tag{2.14.4}$$

$$c^o_{22} = \sin\theta_o \sin\psi_o \sin\phi_o + \cos\psi_o \cos\phi_o \tag{2.14.5}$$

$$c^o_{23} = \cos\theta_o \sin\psi_o \tag{2.14.6}$$

$$c^o_{31} = \sin\theta_o \cos\psi_o \cos\phi_o + \sin\psi_o \sin\phi_o \tag{2.14.7}$$

$$c^o_{32} = \sin\theta_o \cos\psi_o \sin\phi_o - \sin\psi_o \cos\phi_o \tag{2.14.8}$$

$$c^o_{33} = \cos\theta_o \cos\psi_o \tag{2.14.9}$$

A geometric interpretation of the Euler angles used in this work can be found in Patrikalakis and Chryssostomidis [7].

To complete the set of governing equations, the constitutive relation between T_o and e_o needs to be used:

$$T_0 = EA\, e_0 \qquad (2.15)$$

In the case of the general three-dimensional static problem $N_0 = 13$ boundary conditions are necessary to complete the statement of the problem. For the case of a buoyant riser configuration, de Oliveira and Morton [11] and de Oliveira et al [12], an appropriate set of boundary conditions involves the prescription of ϕ_0, θ_0, ψ_0, x_0, y_0 and z_0 at s=0 and s=L and $s^*(0)=0$. For the case of a catenary configuration, Panicker and Yancey [13], the above boundary conditions at s=0 need to be modified to also express the equilibrium of interaction forces and moments and kinematic compatibility with the lower rigid riser section.

2.3 External Forces and Moments

The prediction of the external loads $\vec{F}_{Ho}$ and $\vec{M}_{Ho}$ is, perhaps, one of the more important factors in a successful analysis of the static behavior of compliant risers. Until rational methods allow the prediction of these loads in separated flows, approximate estimates based on strip theory and experimental two-dimensional flow models may be used for design purposes, see Patrikalakis [4] and Patrikalakis and Chryssostomidis [8]. Due to lack of appropriate experimental data for compliant riser geometries, we adopt the following procedure based on Sarpkaya and Isaacson [14] to estimate the external static force $\vec{F}_{Ho}$ due to a current. We assume first

that the external current velocity is a given function of y_o and of the following form:

$$\vec{V}(y_o)=[V_x(y_o),0,V_z(y_o)]\cdot U \qquad (2.16)$$

Using equation (2.14) we can estimate the components v_o^{ζ} , v_o^{ξ} and v_o^{η} of $\vec{v}$ in the local $\vec{\zeta}_o$, $\vec{\xi}_o$ and $\vec{\eta}_o$ system at a particular point C on the riser centerline:

$$[V_o^{\zeta},V_o^{\xi},V_o^{\eta}]^T = C_o\cdot[V_x(y_o),0,V_z(y_o)]^T$$

The component of $\vec{v}$ orthogonal to $\vec{\zeta}_o$, denoted by $\vec{v}_o^{\xi\eta}$, can be obtained from:

$$\vec{V}_o^{\xi\eta} = V_o^{\xi}\vec{\xi}_o+V_o^{\eta}\vec{\eta}_o \qquad (2.17)$$

The static drag force perpendicular to $\vec{\zeta}_o$ and in the direction of $\vec{v}_o^{\xi\eta}$ is expressed as:

$$\vec{F}_{Ho}^{\xi\eta} = 0.5\rho_w D_f C_D \vec{V}_o^{\xi\eta}|\vec{V}_o^{\xi\eta}| \qquad (2.18)$$

where D_f is the maximum frontal dimension of the cross-section orthogonal to $\vec{v}_o^{\xi\eta}$ and C_D is a drag coefficient, which depends at least upon the geometry of the cross- section, its orientation and Reynolds number and is primarily due to separation and wake formation. Using (2.17) and (2.18), the drag forces in the directions $\vec{\xi}_o$ and $\vec{\eta}_o$ can be obtained from:

$$F_{Ho}^{\xi} = 0.5\rho_w D_f(s) C_D V_o^{\xi}|\vec{V}_o^{\xi\eta}| \qquad (2.19)$$

$$F_{Ho}^{\eta} = 0.5\rho_w D_f(s) C_D V_o^{\eta}|\vec{V}_o^{\xi\eta}| \qquad (2.20)$$

To simplify our calculations we further assume that we can approximate a compliant riser cross-section as in Figure 2-1 below

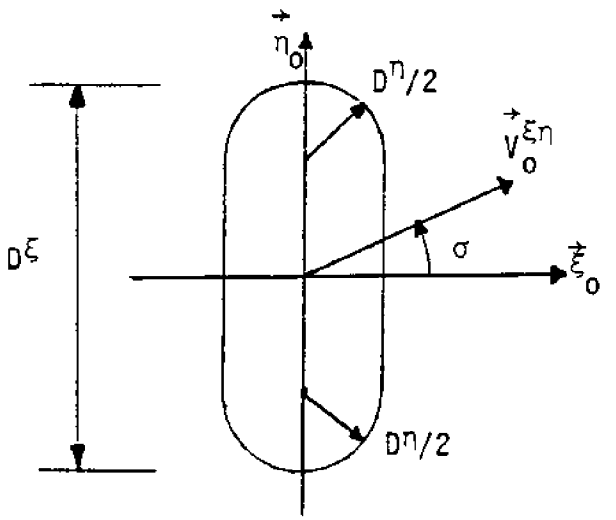

Figure 2-1: Cross-section Idealization

for our estimates of D_f . We observe that the cross-section in Figure 2-1 reduces to a circle if $D^\xi = D^\eta$ and will provide a correct estimate of D_f for an arbitrary number of tubes of equal diameter arranged along the $\vec{n}$ axis consecutively in a series. From the assumed geometry we obtain:

$$D_f=(D^\xi-D^\eta)|\cos\sigma|+D^\eta \qquad (2.21)$$

where

$$|\cos\sigma|=|V_o^\xi|/|\vec{V}_o^{\xi\eta}| \qquad (2.22)$$

Using (2.21) to (2.22), we can reduce (2.19) and (2.20) to

$$F^{\xi}_{Ho} = 0.5\rho_w C_D V^{\xi}_o[(D^{\xi}-D^{\eta})|V^{\xi}_o| + D^{\eta}|\vec{V}^{\xi\eta}_o|] \qquad (2.23)$$

$$F^{\eta}_{Ho} = 0.5\rho_w C_D V^{\eta}_o[(D^{\xi}-D^{\eta})|V^{\xi}_o| + D^{\eta}|\vec{V}^{\xi\eta}_o|] \qquad (2.24)$$

Elongated compliant riser sections are expected to experience a small (static) lift orthogonal to $\vec{\zeta}_o$ and $\vec{V}^{\xi\eta}_o$, which is however neglected in this work due to lack of appropriate experimental data. In all subsequent analysis (2.23) and (2.24) will be used to predict the static forces in the $\vec{\xi}_o$ and $\vec{\eta}_o$ directions respectively. In the numerical implementation, D^{ξ} and D^{η} are functions of s. We can therefore model risers, the cross-sections of which are multiple adjacent tubes in a series possibly covered with circular buoyancy modules over part of their length.

For the evaluation of the drag force parallel to $\vec{\zeta}_o$ we distinguish two separate contributing mechanisms. First, a frictional component which can be evaluated from:

$$F^{f}=0.5\rho_w P^{\xi\eta}(s)C_f V^{\zeta}_o|V^{\zeta}_o| \qquad (2.25)$$

where $P^{\xi\eta}(s)$ is the length of the wetted perimeter of the cross- section and C_f a frictional coefficient which is at least two orders of magnitude less than C_D . Second, we distinguish a separation drag parallel to $\vec{\zeta}_o$ due to presence of buoyancy modules. It is possible to incorporate this effect in an equation which provides the total drag force in the $\vec{\zeta}_o$ direction, while keeping the form of equation (2.25) by writing:

$$F_{Ho}^{\zeta}=0.5\rho_w P_e^{\xi\eta}(s)C_f V_o^{\zeta}|V_o^{\zeta}| \qquad (2.26)$$

where $P_e^{\xi\eta}(s)$ is an "equivalent" wetted perimeter defined by

$$P_e^{\xi\eta}(s)=P^{\xi\eta}(s) + \frac{C_D'(A_b-A_o)}{C_f \cdot L_b} \qquad (2.27)$$

where C_D' is a separation drag coefficient for the buoyancy modules for a flow parallel to ζ_o, A_b, A_o the cross-sectional area of the buoyancy modules and riser tubes and L_b the length of the buoyancy modules. Within the bare part of the compliant riser we can set $A_b = A_o$ and therefore get $P_e^{\xi\eta}(s) = P^{\xi\eta}(s)$ to recover (2.25). Within the part of the riser covered by buoyancy modules, equations (2.26) and (2.27) also allow a uniformly distributed force due to separation.

Finally, we need to provide estimates for the external torque per unit length, M_{Ho}^{ζ}. Within ideal flow theory, the presence of M_{Ho}^{ζ} can be explained because the cross-section is not, in general, symmetrical about an axis orthogonal to $\vec{V}_o^{\xi\eta}$ on the $\xi_o\eta_o$ plane, see Newman [15]. Due to lack of experimental data for real flow conditions, we estimate the external torque per unit length from potential theory, Newman [15], using:

$$M_{Ho}^{\zeta} = (m_a^{\xi} - m_a^{\eta})\, V_o^{\xi} V_o^{\eta} \qquad (2.28)$$

where m_a^{ξ} and m_a^{η} are the added masses per unit length in the $\vec{\xi}_o$ and $\vec{\eta}_o$ directions. The values of the added masses are considered functions of s in our implementation and therefore

allow M^{ζ}_{H0} to become zero for circular cross-sections. Denoting by σ the angle between $\vec{\xi}_0$ and $\vec{V}^{\xi\eta}_0$, equation (2.28) can be reduced to the following form:

$$M^{\zeta}_{Ho}=0.5(m^{\xi}_a-m^{\eta}_a)\sin 2\sigma|\vec{V}^{\xi\eta}_0|^2 \qquad (2.29)$$

This equation indicates that for a particular cross-section and current velocity, the external torque reaches an extremum when $\sigma=(2n-1)\pi/4$ for n=1,2,3,4.

2.4 Non-Dimensional Three-Dimensional Equations

It is convenient to convert the governing equations to a first order system of ordinary differential equations of the following symbolic form:

$$\vec{w}_{os} = \vec{f}_0(s,\vec{w}_0) \qquad (2.30)$$

where $\vec{w}_0(s)$ is the solution vector and $\vec{f}_0$ a given (non-linear) function of $\vec{w}_0$ and s. For the general three-dimensional static problem we choose:

$$\vec{w}_0=[T_0,Q^{\xi}_0,Q^{\eta}_0;\Omega^{\zeta}_0,\Omega^{\xi}_0,\Omega^{\eta}_0;\phi_0,\theta_0,\psi_0;x_0,y_0,z_0;s^*_0]^T \qquad (2.31)$$

with $N_0=$ 13 unknown scalar variables. The first twelve variables are coupled in the governing equations, while $s^*_0(s)$ can be determined from (2.13) and (2.15) once the computation of T_0 is completed.

Before proceeding to bring the governing equations in the form (2.30), it is convenient to introduce non-dimensional variables. Forces are non-dimensionalized by $W_a L$, where W_a is

the average effective weight per unit length of the riser fully submerged in water. Lengths are non-dimensionalized by L the unstretched length of the riser. We also introduce the following non-dimensional parameters:

$$\beta^{p}(s)=W_a L^3/GI^{p}(s) \tag{2.32}$$

$$\beta^{\xi}(s) = W_a L^3/EI^{\xi\xi}(s) \tag{2.33}$$

$$\beta^{\eta}(s) = W_a L^3/EI^{\eta\eta}(s) \tag{2.34}$$

$$\gamma(s) = W_a L/EA(s) \tag{2.35}$$

$$\mu(s,y_o) = W(s,y_o)/W_a \tag{2.36}$$

and from now we denote non-dimensional quantities with the same symbol as dimensional quantities. If we wish to refer to a dimensional quantity, we will state this explicitly. The resulting non-dimensional equations describing three-dimensional statics of a compliant riser with torsion are:

$$T_{os} = \mu c^{o}_{12}+Q^{\xi}_{o}\Omega^{\eta}_{o}-Q^{\eta}_{o}\Omega^{\xi}_{o}-F^{\zeta}_{Ho} \tag{2.37}$$

$$Q^{\xi}_{os} = \mu c^{o}_{22}+Q^{\eta}_{o}\Omega^{\zeta}_{o}-T_{o}\Omega^{\eta}_{o}-F^{\xi}_{Ho} \tag{2.38}$$

$$Q^{\eta}_{os} = \mu c^{o}_{32} + T_o \Omega^{\xi}_o - Q^{\xi}_o \Omega^{\zeta}_o - F^{\eta}_{Ho} \tag{2.39}$$

$$\Omega^{\zeta}_{os} = -\beta^{p}[M^{\zeta}_{Ho} + (1/\beta^{\eta} - 1/\beta^{\xi})\Omega^{\eta}_o \Omega^{\xi}_o + (1/\beta^{p})_s \Omega^{\zeta}_o] \tag{2.40}$$

$$\Omega^{\xi}_{os} = \beta^{\xi}[Q^{\eta}_o - (1/\beta^{p} - 1/\beta^{\eta})\Omega^{\zeta}_o \Omega^{\eta}_o - (1/\beta^{\xi})_s \Omega^{\xi}_o] \tag{2.41}$$

$$\Omega^{\eta}_{os} = -\beta^{\eta}[Q^{\xi}_o - (1/\beta^{p} - 1/\beta^{\xi})\Omega^{\xi}_o \Omega^{\zeta}_o + (1/\beta^{\eta})_s \Omega^{\eta}_o] \tag{2.42}$$

$$\phi_{os} = (\Omega^{\xi}_o \sin\psi_o + \Omega^{\eta}_o \cos\psi_o)/\cos\theta_o \tag{2.43}$$

$$\theta_{os} = \Omega^{\xi}_o \cos\psi_o - \Omega^{\eta}_o \sin\psi_o \tag{2.44}$$

$$\psi_{os} = \Omega^{\zeta}_o + \tan\theta_o[\Omega^{\xi}_o \sin\psi_o + \Omega^{\eta}_o \cos\psi_o] \tag{2.45}$$

$$x_{os} = (1+\gamma T_o)c^{o}_{11} \tag{2.46}$$

$$y_{os} = (1+\gamma T_o)c^{o}_{12} \tag{2.47}$$

$$z_{os} = (1+\gamma T_o)c^{o}_{13} \tag{2.48}$$

$$s^{*}_{os} = 1+\gamma T_o \tag{2.49}$$

where the elements c^{o}_{ij} of the static transformation matrix can be evaluated from (2.14) in terms of the Euler angles.

The boundary conditions appropriate for a buoyant riser configuration, such as in de Oliveira and Morton [11], are:

$$x_o(0)=y_o(0)=z_o(0) = s^*_o(0) = 0 \tag{2.50}$$

$$\theta_o(0) = \psi_o(0) = 0 \tag{2.51}$$

$$\phi_o(0) = \phi_B \tag{2.52}$$

$$x_o(l)=x_T;\ y_o(l)=y_T;\ z_o(l)=z_T \tag{2.53}$$

$$\phi_o(l)=\phi_T;\ \theta_o(l)=\theta_T;\ \psi_o(l)=\psi_T \tag{2.54}$$

2.5 Non-Dimensional Two-Dimensional Equations Without Torsion

In this case the solution vector (2.31) reduces to $N_o = 7$ non-trivial components:

$$\vec{w}_o = [T_o, Q^{\xi}_o; \Omega^{\eta}_o; \phi_o; x_o, y_o; s^*_o]^T \tag{2.55}$$

The non-dimensional governing equations describing the two-dimensional static problem without torsion in the $\vec{i}$ $\vec{j}$ plane obtained from (2.37) to (2.49) using (2.14) are:

$$T_{os} = \mu \sin\phi_o + Q^{\xi}_o \Omega^{\eta}_o - F^{\xi}_{Ho} \tag{2.56}$$

$$Q^{\xi}_{os} = \mu \cos\phi_o - T_o \Omega^{\eta}_o - F^{\xi}_{Ho} \tag{2.57}$$

$$\Omega^{\eta}_{os} = -\beta^{\eta}[Q^{\xi}_{o} + (1/\beta^{\eta})_{s}\Omega^{\eta}_{o}] \tag{2.58}$$

$$\phi_{os} = \Omega^{\eta}_{o} \tag{2.59}$$

$$x_{os} = (1+\gamma T_{o})\cos\phi_{o} \tag{2.60}$$

$$y_{os} = (1+\gamma T_{o})\sin\phi_{o} \tag{2.61}$$

$$s^{*}_{os} = 1+\gamma T_{o} \tag{2.62}$$

The boundary conditions appropriate for a buoyant riser configuration, such as in de Oliveira and Morton [11], are:

$$x_{o}(0) = y_{o}(0) = s^{*}_{o}(0) = 0 \tag{2.63}$$

$$\phi_{o}(0) = \phi_{B} \tag{2.64}$$

$$x_{o}(1) = x_{T},\ y_{o}(1) = y_{T} \tag{2.65}$$

$$\phi_{o}(1) = \phi_{T} \tag{2.66}$$

In the two-dimensional case, the $\vec{\zeta}_{o}$ and $\vec{\xi}_{o}$ components of the external force due to current $\vec{V}(y_{o}) = V_{x}(y_{o})\vec{I}$ reduce to:

$$F_{Ho}^{\zeta} = \kappa_f \cos\phi_o |\cos\phi_o| \tag{2.67}$$

$$F_{Ho}^{\xi} = -\kappa \sin\phi_o |\sin\phi_o| \tag{2.68}$$

where:

$$\kappa_f(s,y_o) = 0.5\rho_w p_e^{\xi\eta}(s) C_f V_x(y_o)|V_x(y_o)|/W_a \tag{2.69}$$

$$\kappa(s,y_o) = 0.5\rho_w D^{\xi}(s) C_D V_x(y_o)|V_x(y_o)|/W_a \tag{2.70}$$

Chapter 3

NUMERICAL SOLUTION ALGORITHM

3.1 Introduction

General methods for the solution of two-point boundary value problems can be found in Keller [16], Ferziger [17] and Pereyra [18]. We start our discussion from the solution of the general three-dimensional static problem with torsion described by equations (2.37) to (2.49). In this work, we solve equations (2.37) to (2.49), supplemented by boundary conditions (2.50) to (2.54), by embedding our problem into a more general class of boundary value problems. Symbolically our problem:

$$\vec{w}' = \vec{f}(s,\vec{w}),\ \vec{g}[\vec{w}(0),\vec{w}(1)] = 0 \qquad (3.71)$$

where prime denotes derivative with respect to s,

$\vec{w}=[w_1(s),w_2(s)\ldots w_N(s)]^T$ is the solution vector,

$\vec{f}=[f_1,f_2\ldots f_N]^T$, $\vec{g}=[g_1,g_2\cdots g_N]^T$,

$0\leq s\leq 1$, and $[\ ]^T$ denotes transpose

is embedded into

$$\vec{w}'=\vec{f}(s,\vec{w};\varepsilon),\ \vec{g}[\vec{w}(0),\vec{w}(l);\varepsilon]=0 \tag{3.72}$$

where ε is a continuation parameter, $0\leq\varepsilon\leq 1$, and when $\varepsilon=1$ equations (2.71) and (2.72) are identical.

Using the embedding technique, a sequence of problems with values of ε such that $0=\varepsilon_1<\varepsilon_2\ldots<\varepsilon_p=1$ are solved. The solution of the problem involving ε_k uses as initial approximation the solution of the problem involving ε_{k-1}.

In our embedding technique for the case of a buoyant riser configuration in a general current, we replace

- equation (2.16) by

$$\vec{V}(y_o;\varepsilon)=[V_{xi}(y_o)+\varepsilon(V_x(y_o)-V_{xi}(y_o)),0,V_{zi}(y_o)+\varepsilon(V_z(y_o)-V_{zi}(y_o))]\cdot U \tag{3.73}$$

equation (2.52) by

$$\phi_o(0;\varepsilon)=\phi_{Bi}+\varepsilon(\phi_B-\phi_{Bi}) \tag{3.74}$$

equations (2.53) by

$$x_o(1;\varepsilon)=x_{Ti}+\varepsilon(x_T-x_{Ti}) \tag{3.75.1}$$

$$y_o(1;\varepsilon)=y_{Ti}+\varepsilon(y_T-y_{Ti}) \tag{3.75.2}$$

$$z_o(1;\varepsilon)=z_{Ti}+\varepsilon(z_T-z_{Ti}) \tag{3.75.3}$$

and equations (2.54) by

$$\phi_o(1;\varepsilon) = \phi_{Ti}+\varepsilon(\phi_T-\phi_{Ti}) \qquad (3.76.1)$$

$$\theta_o(1;\varepsilon) = \theta_{Ti}+\varepsilon(\theta_T-\theta_{Ti}) \qquad (3.76.2)$$

$$\psi_o(1;\varepsilon) = \psi_{Ti}+\varepsilon(\psi_T-\psi_{Ti}) \qquad (3.76.3)$$

where subscript i denotes an initial problem, $\varepsilon=0$, for which the full solution of the corresponding boundary value problem is available. This solution may, for example, be the result of a previous step of our procedure. We also note that by selecting V_{zi} , z_{Ti} , θ_{Ti} and ψ_{Ti} to be zero, the resulting initial problem, $\varepsilon=0$, is a two- dimensional static problem without torsion, which is relatively simpler to solve. We, therefore, see that we can start the solution of the general three- dimensional problem from the solution of the two-dimensional problem which we treat next. Solutions of this problem, with the method explained in the sequel have been published by Chryssostomidis and Patrikalakis [19].

In our embedding technique for the case of a two-dimensional configuration of a buoyant riser (in the $\vec{i}$ $\vec{j}$ plane) in a moderate to strong current in the x direction, we replace

$V_x(y_o)|V_x(y_o)|$ in equations (2.69) and (2.70) by

$$\bar{V}_x|\bar{V}_x| + \varepsilon[V_x(y_o)|V_x(y_o)| - \bar{V}_x|\bar{V}_x|]$$

where $\bar{V}_x$ is the mean current speed of the original problem

- μ in equations (2.56) and (2.57) by $\varepsilon\mu$, and
- x_T and y_T in equations (2.65) by $x'_T + \varepsilon(x_T - x'_T)$ and $y'_T + \varepsilon(y_T - y'_T)$, where x'_T and y'_T are defined in Section 3.2.

In this manner, we obtain an initial problem, $\varepsilon=0$, which

- is easier to solve than the actual problem ($\varepsilon=1$), so we can start our solution process without difficulty, see Section 3.2, and
- expresses the balance of all major external and restoring forces of the original problem correctly, everywhere in $0 \leq s \leq 1$.

For the case of a buoyant riser in a moderate to strong current, the major external force is the normal drag, and the major restoring force is the effective tension except near the ends where bending becomes also important. Using our embedding technique, we obtain an initial problem, $\varepsilon=0$, which corresponds to a neutrally buoyant riser in a moderate to strong constant current. This idealization, therefore, gives us a correct estimate of the order of magnitude of both external and restoring forces.

For the case of a buoyant riser in a weak or zero current our embedding technique involves the following steps:

- we determine the response of the actual riser in a fictitious moderate constant current, V_{xi} , using the procedure outlined above, and
- we replace $V_x(y_o)|V_x(y_o)|$ in equations (2.69) and (2.70) by

$$V_{xi}|V_{xi}| + \varepsilon[V_x(y_o)|V_x(y_o)| - V_{xi}|V_{xi}|]$$

In the case of a weak current the two step process is necessary in order to determine an initial configuration for the second step which includes the effects of effective weight, which now plays a significant role.

The solution of equation (3.72) was obtained using a non-uniform grid finite difference method, see Pereyra [18]. The non-uniform grid was necessary to permit an efficient resolution of boundary layers near s=0 and s=1, see Patrikalakis [4]. The solution of the finite difference equations is based on a modified Newton's iteration method coupled with a deferred correction technique also described in Pereyra [18]. This method uses an approximate solution of the problem and yields a more accurate solution which makes the absolute error less than a prespecified tolerance. During the solution process, additional grid points may be inserted automatically to reduce and to equidistribute the error on the final mesh. Our code uses the Fortran library NAG [20] and has been implemented on an IBM 370/168 mainframe. All arithmetic was done in double precision (15 decimal digits).

3.2 Initial Asymptotic Approximation of the Two-Dimensional Solution

In this Section, we derive an approximate solution of the two- dimensional static problem for $\varepsilon=0$ corresponding to a neutrally buoyant compliant riser in a constant current. For simplicity we neglect frictional forces because of their small effect in the determination of effective tension. In addition

we use the mean frontal diameter, $\bar{D}^{\xi}$, in the estimation of the normal drag force. Finally we assume that $\gamma=0$ because the extensional rigidity of the riser is very large. With these assumptions the resulting governing equations are:

$$T_{os} = Q_o^{\xi}\,\Omega_o^{\eta},\quad Q_{os}^{\xi} = -T_o\Omega_o^{\eta} + \kappa\sin^2\phi_o \tag{3.77}$$

$$\Omega_{os}^{\eta} = -\beta^{\eta}[Q_o^{\xi}+(1/\beta^{\eta})_s\Omega_o^{\eta}],\quad \phi_{os} = \Omega_o^{\eta} \tag{3.78}$$

$$x_{os} = \cos\phi_o,\quad y_{os} = \sin\phi_o \tag{3.79}$$

where

$$\kappa = 0.5\rho_w\bar{D}^{\xi}C_D\,\bar{V}_x|\bar{V}_x|/W_a \tag{3.80}$$

A uniform leading order approximation of $\phi_o(s)$ can be found by simple boundary layer theory, see Carrier and Pearson [21], to be

$$\phi_o(s) \simeq \phi_o^0(s) + \phi_o^1(s)+\phi_o^2(s) \tag{3.81}$$

where

$$\phi_o^0(s) = \text{Arctan}[-1/(\lambda s+c)]+\delta \tag{3.82}$$

$$\phi_o^1(s) = [\phi_B-\phi_o^0(0)]\exp\{-s[\bar{T}_o\beta^{\eta}(0)]^{1/2}\} \tag{3.83}$$

$$\phi_0^2(s) = [\phi_T - \phi_0^0(1)]\exp\{-(1-s)[\bar{T}_0\beta^\eta(1)]^{1/2}\} \qquad (3.84)$$

$$\delta=0 \text{ if } -(\lambda s+c)\geq 0,\ \delta=\pi \text{ if } -(\lambda s+c)<0 \qquad (3.85)$$

$$\lambda = \kappa/\bar{T}_0 \qquad (3.86)$$

c is a constant of integration and $\bar{T}_0$ the leading order estimate of the tension, which in our case is independent of s.

Imposing the boundary conditions (2.65) and neglecting the contributions of $\phi_0^1(s)$ and $\phi_0^2(s)$, because they are small, we obtain

$$(1/\lambda)[1/\sin\phi_0^0(0) - 1/\sin\phi_0^0(1)] - x_T = 0 \qquad (3.87)$$

$$(1/\lambda)\ln\{\tan[\phi_0^0(1)/2]/\tan[\phi_0^0(0)/2]\} - y_T = 0 \qquad (3.88)$$

Equations (3.86) to (3.88) are three algebraic equations for λ, c and $\bar{T}_0$ which are solved by Powell's hybrid method, see Powell [22] and therefore equation (3.81) is now fully determined. This in turn allows us to obtain leading order approximations for T_0, Q_0^ξ, Ω_0^η, x_0 and y_0. When we integrate equations (3.79) using (3.81), we obtain $x_0(1)=x_T'$ and $y_0(1)=y_T'$

where x_T' and y_T' are close to but not identical to x_T and y_T . This small discrepancy is rectified by our embedding procedure in which we replace x_T by $x_T' + \epsilon (x_T - x_T')$ and y_T by $y_T' + \epsilon (y_T - y_T')$.

Chapter 4

NUMERICAL RESULTS FOR A BUOYANT RISER CONFIGURATION WITH UNIFORMLY DISTRIBUTED BUOYANCY MODULES

The structural design details of the buoyant compliant riser analyzed in this work can be found in de Oliveira and Morton [11]. The riser is made up of two flexible tubes with inner diameter of 85.7 mm and outer diameter of 122.9 mm, clamped together as in Figure 4-1 .

The overall riser characteristics are: L=88.392 m; $W=W_a$=2.92 N/m; EA=267 MN; $EI^{\eta\eta}$ =3.3 kN.m^2; $EI^{\xi\xi}$ =12.2 kN.m^2; GI^P=0.582 MN.m^2; D^{ξ}=0.31 m; D^{η}=0.20 m; $P_e^{\xi\eta}$ =0.93 m; A_0=237.4 cm^2; A_i=115.4 cm^2; ρ_i=820 kg/m^3; p=3.45 MPa; c=0; m=49.93 kg/m; m^{ζ}=40.47 kg/m; m_a^{ξ} =82.44 kg/m; m_a^{η} =50.32 kg/m; vertical distance of lower support, s=0, from ocean floor is 7.62 m. The value of the effective weight was taken constant because it was assumed that buoyancy is provided by small uniformly distributed modules, Patrikalakis [4]. If this is not the case the local value of W should be used. For the same reason, effective constant values of D^{ξ}, D^{η}, $P_e^{\xi\eta}$, m, m^{ζ}, m_a^{ξ} and m_a^{η} are used in this paper. Due to presence of strain relief units at the ends, the following values of bending and torsional rigidities at s=0 and s=L were used: $EI^{\eta\eta}$ =6.6

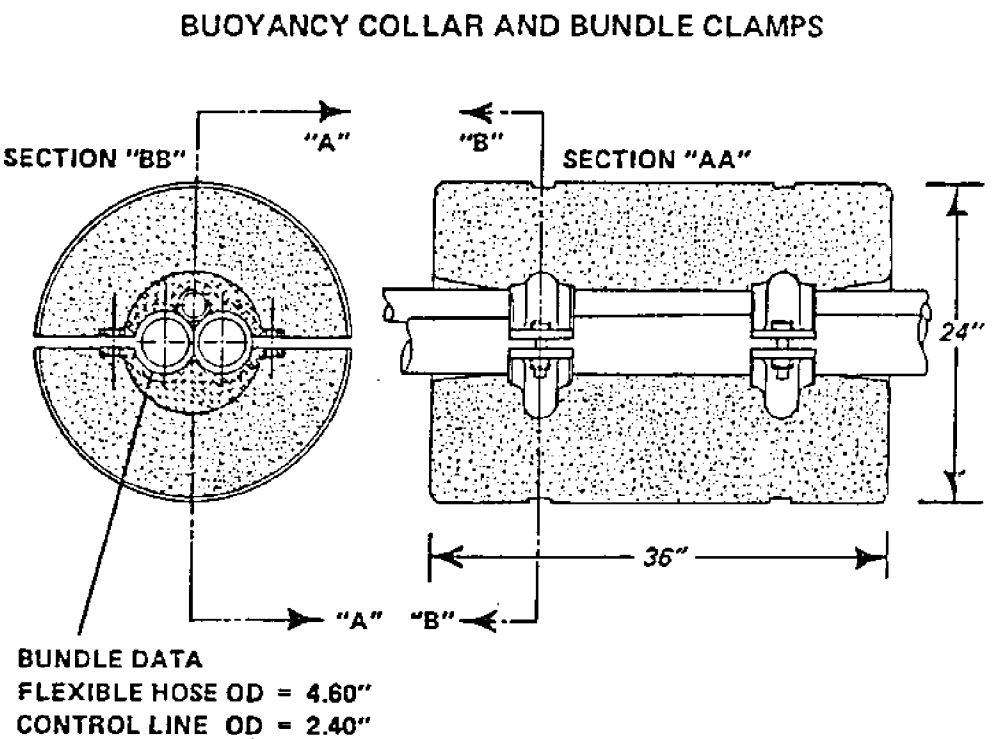

Figure 4-1: Buoyant Compliant Riser Concept Proposed In [11]

$kN.m^2$; $EI^{\xi\xi}$ =24.4 $kN.m^2$; GI^P=1.164 $MN.m^2$. These rigidities were assumed to decay linearly to the previous values within 10 m from s=0 and s=L. In addition, for all excitation conditions studied in this paper we used $\phi_B = \phi_T = 90$ degrees; $\theta_T = 0$; $z_T = 0$; and $C_D = 1$ and $C_f = 0.05$.

The excitation cases we investigate in this paper correspond to the expected minimum and maximum water depth for the application described in de Oliveira and Morton [11]. In Case 1, the water depth was 80.77 m; $h_w=h_i$=73.15 m; x_T=0 and y_T=70.10 m. In Case 2, the water depth was 92.96 m; $h_w=h_i$=85.34 m; x_T=6.10 m and y_T=82.30 m. For Case 1, two two-dimensional and four three-dimensional excitation conditions were examined. Condition 1 involves two-dimensional excitation (without torsion) by a unidirectional linear strong current with $V_x(0)$=1.03 m/s and $V_x(h_w)$=1.55 m/s. In this condition, $\psi_0(L)=0$, leading to a two-dimensional configuration without torsion. Condition 2 corresponds to $\psi_0(L)=0$ and a zero current and represents a "buckled" two-dimensional configuration of the riser due to its own weight in the XY plane. Figures 4-2 and 4-3 show the results of Case 1, Condition 1 and Figures 4-4 and 4-5 the results of Case 1, Condition 2, obtained by executing our two-dimensional static program. For Case 1, Condition 1, the initial approximation for our embedding technique was obtained using the method of Section 3.2 for a constant current equal to 1.29 m/s, the mean value of the actual current. For Case 1, Condition 2, the initial approximation for our embedding

technique was obtained using the method of Section 3.2 for a weak constant current equal to 0.1 m/s. Our embedding procedure, in both cases slowly applies the effective weight forces and modifies the current to the actual profile (linear and zero current, respectively). Figures 4-2 and 4-4 show the displacement x_0 (solid line) and the angle ϕ_0 (dashed line) as a function of y_0. Figures 4-3 and 4-5 show the component of the rate of rotation Ω_0^n (solid line) and the effective tension T_0 (dashed line) as a function of y_0. All variables plotted are non-dimensional.

In Case 1, Condition 1 we observe the creation of sharp boundary layers, the extent of which can be clearly seen from the plot of ϕ_0 versus y_0 , Figure 4.2 . Inside these layers, the effective tension, T_0 , and the component of the rate of rotation, Ω_0^n , change very rapidly while for the remainder of the riser length these two quantities are practically constant as can be seen from Figure 4.3 . Effective tension outside the boundary layers remains essentially constant, because, as we said earlier, our system is highly buoyed. The curvature, Ω_0^n , outside the boundary layers remains essentially constant because the effective tension and external force exhibit small variations with s. The maximum effective tension for Case 1, Condition 1 has been estimated to be 7.974 kN and the maximum tension 47.1 kN. The tension due to internal overpressure amounts to 39.8 kN which shows the importance of the internal overpressure in the estimation of tension. Note, however, that tensile strain is directly related to effective tension,

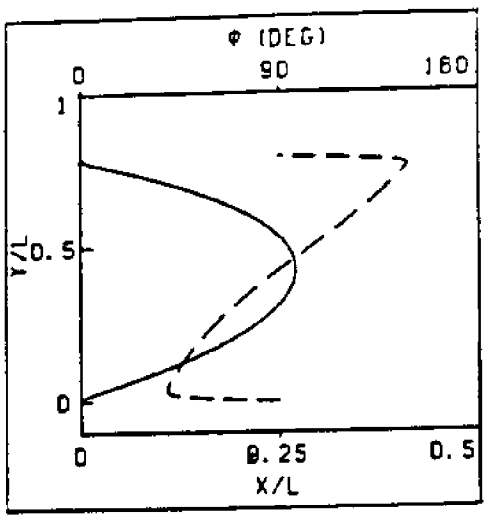

Figure 4-2: x_o, ϕ_o Versus y_o For Case 1 , Condition 1

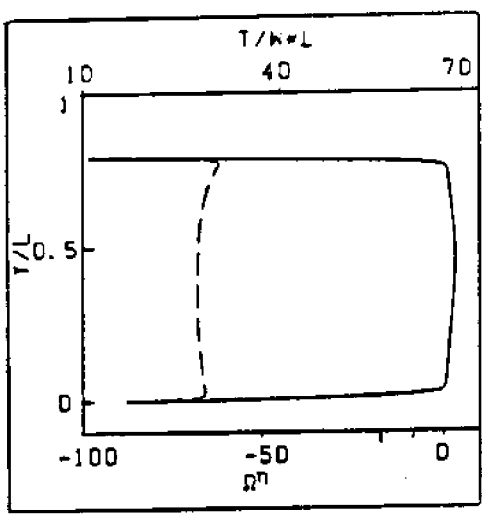

Figure 4-3: Ω_o^{η}, T_o Versus y_o For Case 1 , Condition 1

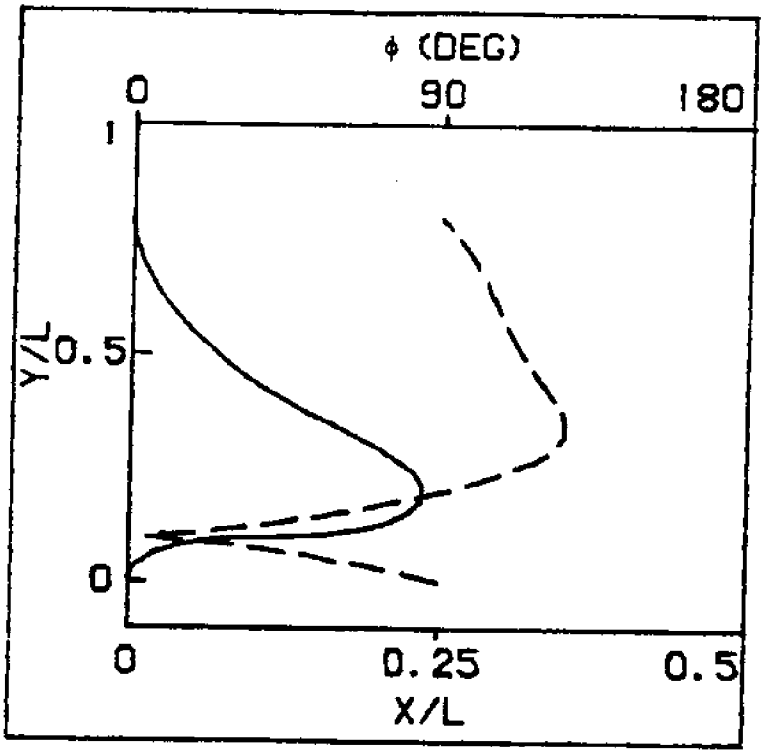

Figure 4-4: x_o, ϕ_o Versus y_o For Case 1 , Condition 2

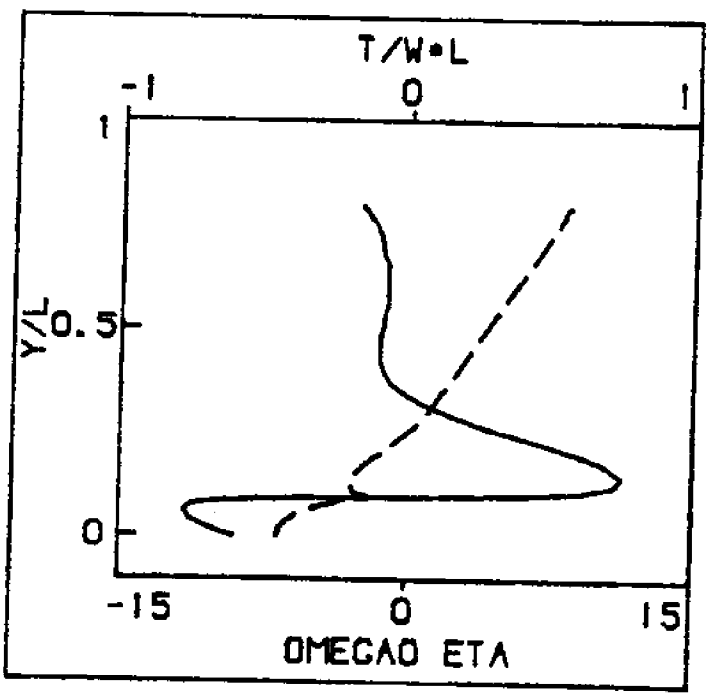

Figure 4-5: Ω_0^{Π}, T_0 Versus y_o For Case 1 ,Condition 2

see equation (2.15), and, therefore, internal overpressure affects hoop stresses primarily, at least within the assumptions of equation (2.15). For a discussion of these assumptions see Appendix C, Patrikalakis and Chryssostomidis [7]. The minimum bending radius for Case 1, Condition 1 is 0.90 m. The value of the minimum bending radius is an important design parameter because it affects the structural integrity of the riser and our ability to access the well, so care must be taken to select the appropriate strain relief units to control bending at the ends.

In Case 1, Condition 2, we observe the creation of a moderately sharp internal layer around s=0.16 where the bending moment rapidly undergoes change of sign and reaches an extreme value. The corresponding minimum bending radius is 7.65 m which is much less critical than the bending radius encountered in Case 1, Condition 1 involving a strong current. This occurs because the value of the effective weight is very small. However, the riser is nearly horizontal within the internal layer referred to above and this may affect our ability to easily access the well. The amount and distribution of buoyancy and the top offset are the important parameters in the present condition of zero current and can be used to control the configuration of the riser. In particular, the effect of non-uniform buoyancy distribution may be studied, with the objective of keeping the riser as vertical as possible for the condition of zero external current. As can be seen from Figure 4-5, the effective

tension varies between $-0.4453\ W_a L$ or 0.12 kN at s=0 and $0.5547\ W_a L$ or 0.14 at s=L becoming positive near s=0.39. The maximum tension occurs at s=L and is equal to 39.5 kN and is almost entirely due to the internal pressure.

For the water depth of Case 1, and in addition to the two two-dimensional static configurations, we also studied the effect of rotating the linear current of Condition 1 to Θ_c =12, 30, 60 and 90 degrees with respect to the XY plane (i.e. from the +X to the -Z direction) with a corresponding platform rotation $\psi_0(L)$=10, 25, 25 and 25 degrees. The solution for the first three-dimensional excitation condition (Θ_c =12 and $\psi_0(L)$=10 degrees) was obtained using the two-dimensional solution for Case 1, Condition 1 as our initial approximation for the starting-up of the embedding procedure. The solution for the next three-dimensional excitation condition (Θ_c =30 and $\psi_0(L)$=25 degrees) was obtained using the previous three-dimensional solution as our initial approximation and so on. The results of our three-dimensional excitation conditions are shown in Figures 4-6 to 4-15 . In Figures 4-6 and 4-7 we plot x_0 and z_0 versus y_0 , respectively. In Figure 4-8 we plot x_0 versus z_0. In Figures 4-9 to 4-11 we plot ϕ_0, θ_0 and ψ_0 versus y_0, respectively. In Figure 4-12 we plot T_0 versus y_0 and in Figures 4-13 to 4-15, Ω_0^{ζ} , Ω_0^{ξ} and Ω_0^{η} versus y_0. All variables plotted are non-dimensional. From Figures 4-6 to 4-8 , we observe that away from the ends the riser nearly follows the direction of the current and its centerline is fairly close to a planar curve. This occurs

because the rigidity of this configuration is very small away from the ends. However, close to the ends Figures 4-6 to 4-11 indicate that the centerline is a highly tortuous curve. This complicated transition near the ends is due to the effects of the boundary conditions and the rigidity of the structure. In Figures 4-6 and 4-8, we can see that when Θ_c=90 degrees (i.e. the current is in the YZ plane), the riser does not lie on the YZ plane, (x_0=0), because of the effect of the top end boundary condition ($\psi_0(L)$=25 degrees). The riser, however, is nearly parallel to the current direction away from the ends. In conclusion, the highly buoyant riser under study readjusts its configuration in response to changes of the direction of the principal external load, i.e. the current, rather than resist this change. This is an indication of its high flexibility. Figures 4-9 to 4-11 clearly indicate the extent of boundary layers near the ends, where bending effects are as important as tension effects. Inside the boundary layer regions, the effective tension T_0 (Figure 4-12), and the components of $\vec{\Omega}$ (Figures 4-13 to 4-15) change very rapidly while for the remainder of the riser these quantities are slowly varying and nearly constant. The effective tension outside the boundary layers remains fairly constant for the same reason as in the two-dimensional configuration. However, this constant value decreased with changing current direction, from Θ_c=10 to 90 degrees because the projected riser area perpendicular to the current direction decreases. For example, looking at cross-sections near s=0.5 where ϕ_0=90

degrees and θ_0=0, we obtain $\psi_0(0.5)$=6.4, 16.0, 20.4 and 16.9 degrees. In this case $\psi_0(0.5)$ represents rotation angle from the XY plane and therefore the relative rotation of the current with respect to the cross-section is 5.6, 14, 39.4 and 73.1 degrees which together with Figure 2-1 provides an explanation of the decrease of the projected area. Figure 4-13 for Ω_0^ζ indicates that the maximum torsion Ω_0^ζ , occurs when Θ_c =60 degrees, or for a relative rotation between current and most cross-sections close to 45 degrees, where the torque due to the current is maximum. However, the resuting maximum shear stress due to torsion is small, as expected from order of magnitude estimates, and is not a critical parameter in this case. Figures 4-14 and 4-15 show that as the current direction changes from Θ_c =0 to 90 degrees, Ω_0^ξ and Ω_0^η near the ends increase and decrease, respectively. The boundary conditions and the change of current direction provide an immediate explanation of this change. The bending strain, ε^b , in a general three-dimensional configuration can be found easily from $\varepsilon^b = \Omega^\xi\eta - \Omega^\eta\xi$, where ξ and η are the non-dimensional local coordinates of a point of a cross section within the material layers participating in bending. So, for example, the maximum bending strain at s=L for Case 1, Condition 1 (two-dimensional configuration) is 0.068 while for Case 1 and the three-dimensional configuration with Θ_c =90 and $\psi_0(L)$=25 degrees the corresponding value is 0.065. The decrease in the maximum bending strain between the two excitation conditions is due to the decrease of the overall

drag due to a decrease of the projected area perpendicular to the current.

Figure Legend (Figures 4-6 to 4-15)

	θ_c	$\psi(L)$ (in degrees)
————	12	10
- - - - - - -	30	25
— — — —	60	25
— - — - —	90	25

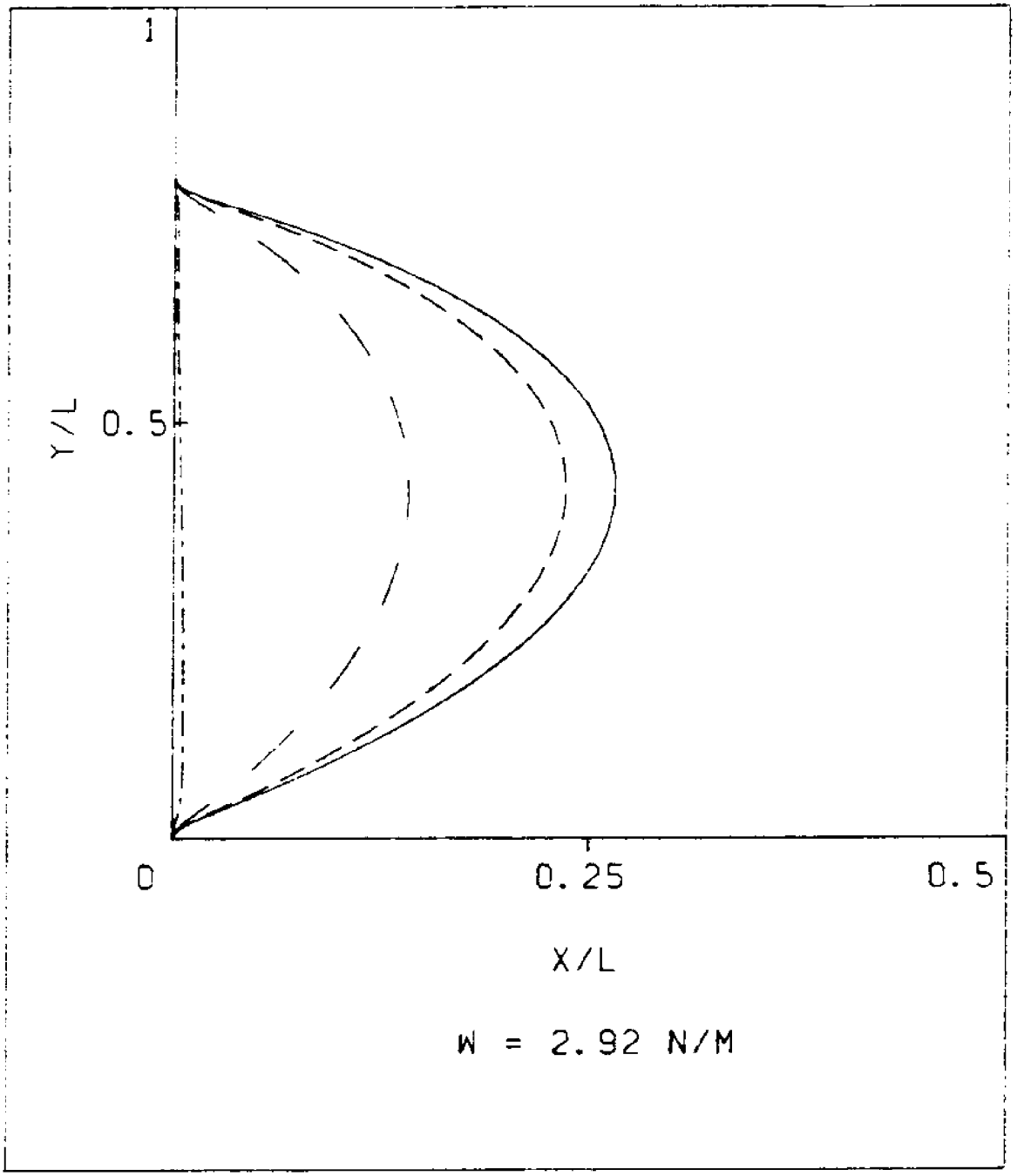

Figure 4-6: x_o Versus y_o For Case 1 And Four 3-D Excitation Conditions

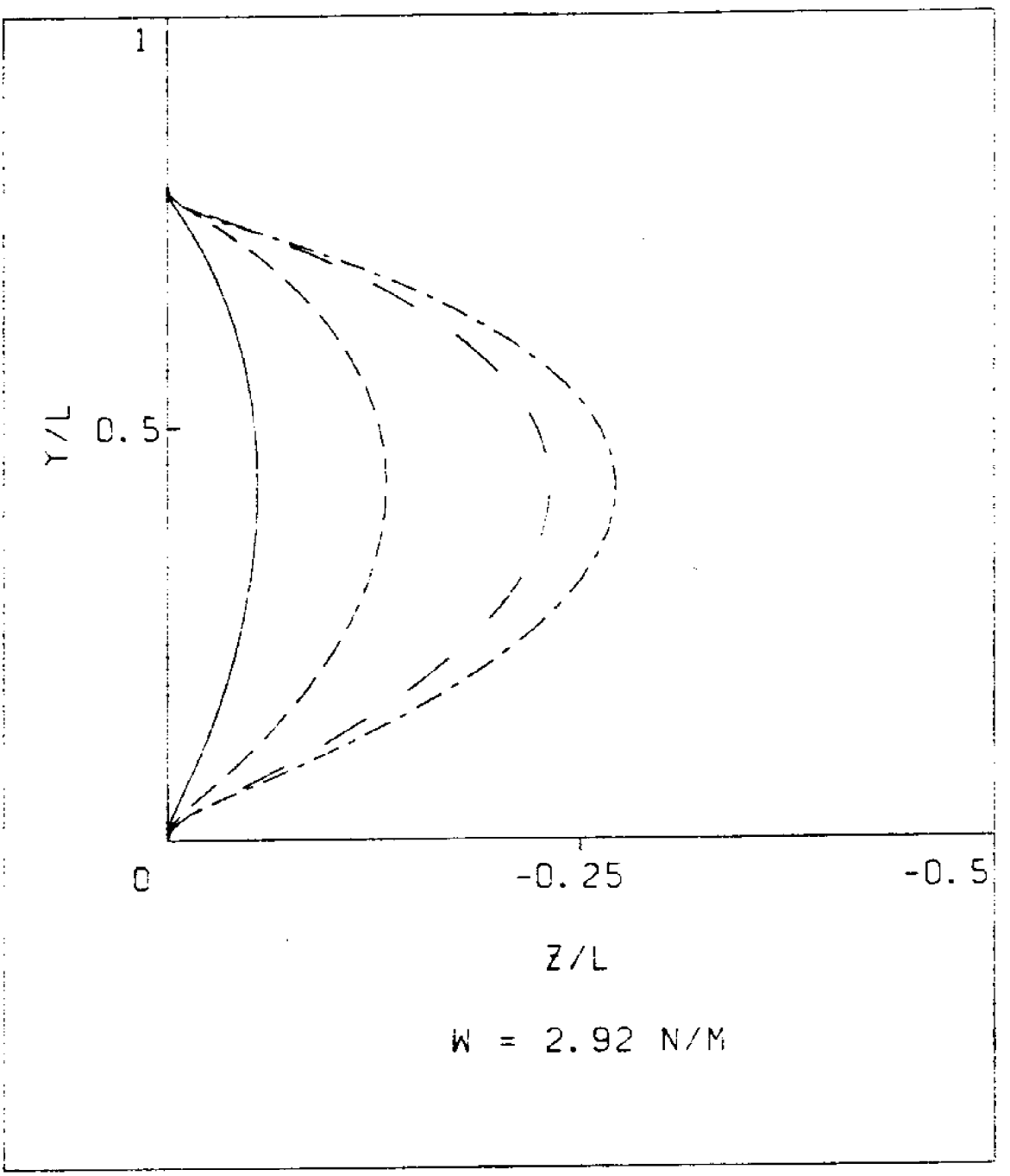

Figure 4-7: z_0 Versus y_0 For Case 1 And Four 3-D Excitation Conditions

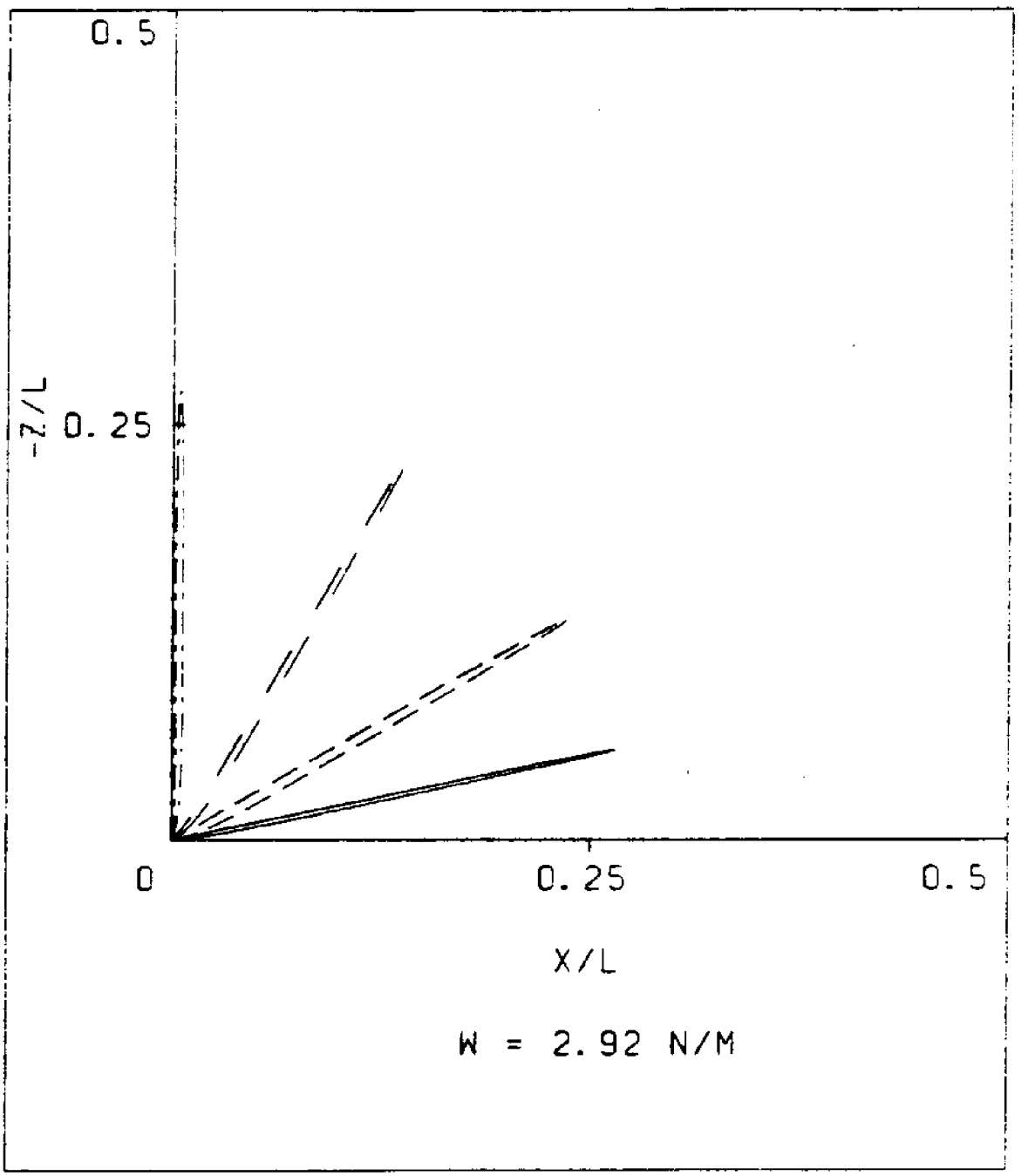

Figure 4-8: x_0 Versus z_0 For Case 1 And Four 3-D Excitation Conditions

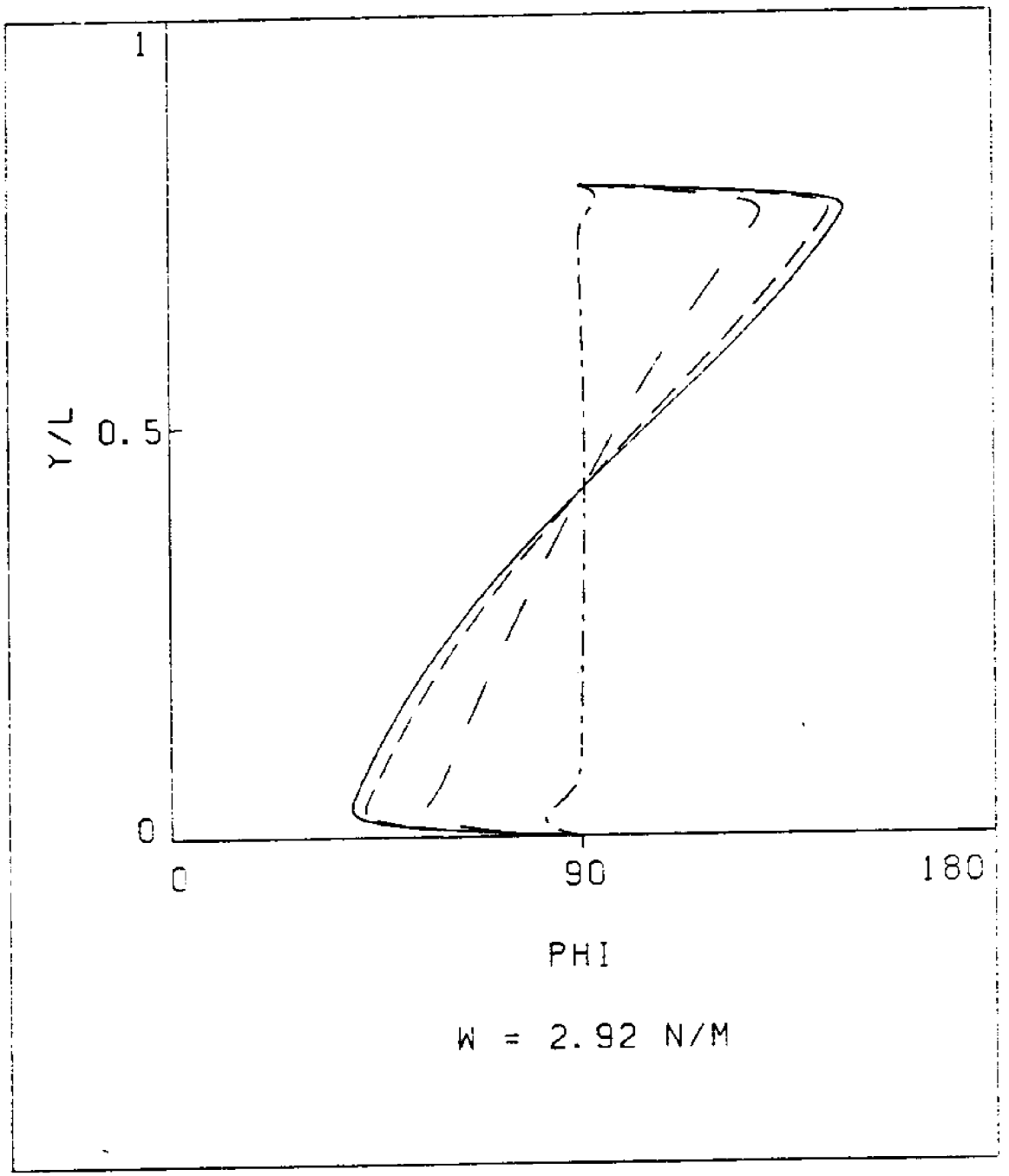

Figure 4-9: ϕ_0 Versus y_0 For Case 1 And Four 3-D Excitation Conditions

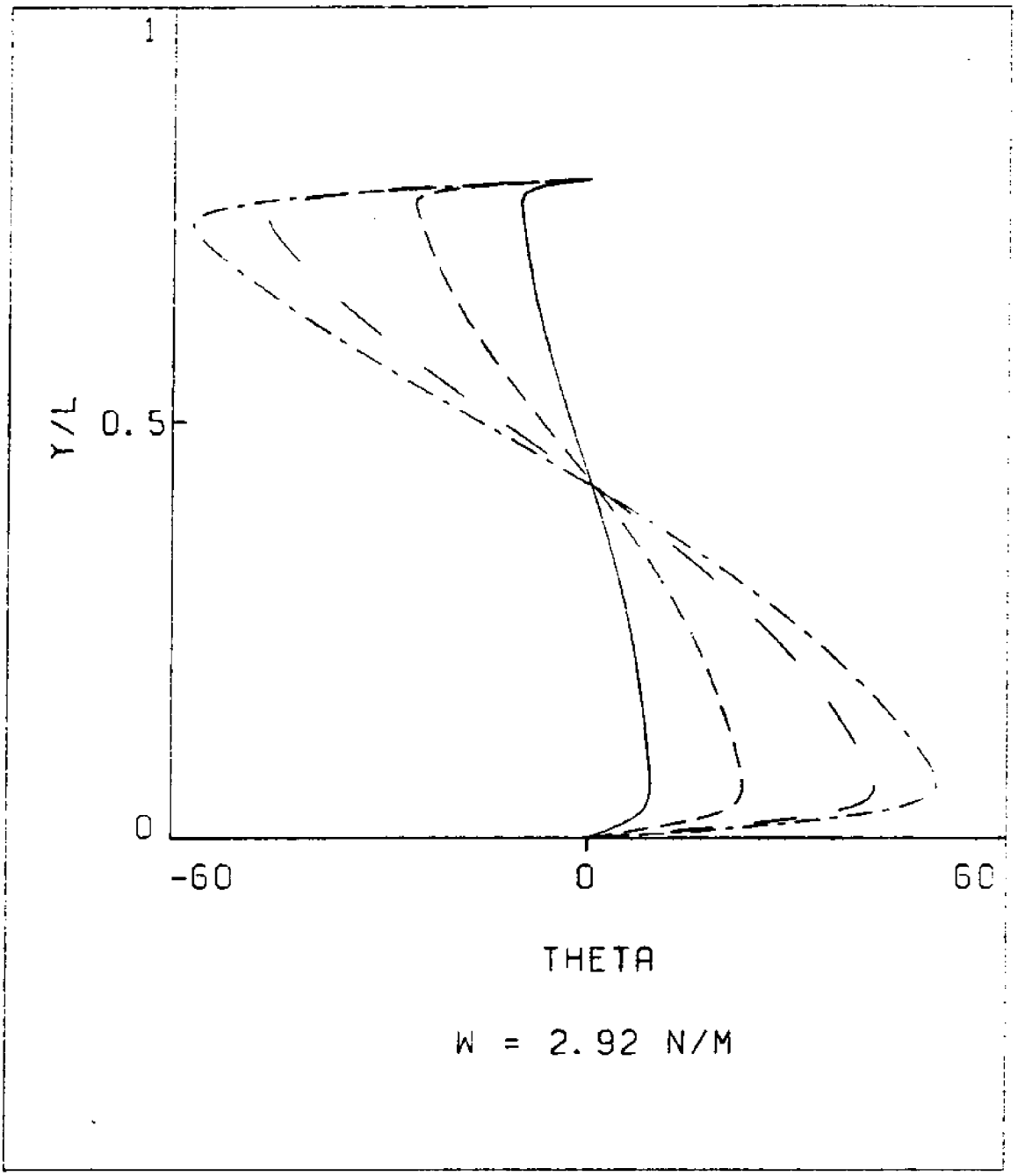

Figure 4-10: θ_0 Versus y_0 For Case 1 And Four 3-D Excitation Conditions

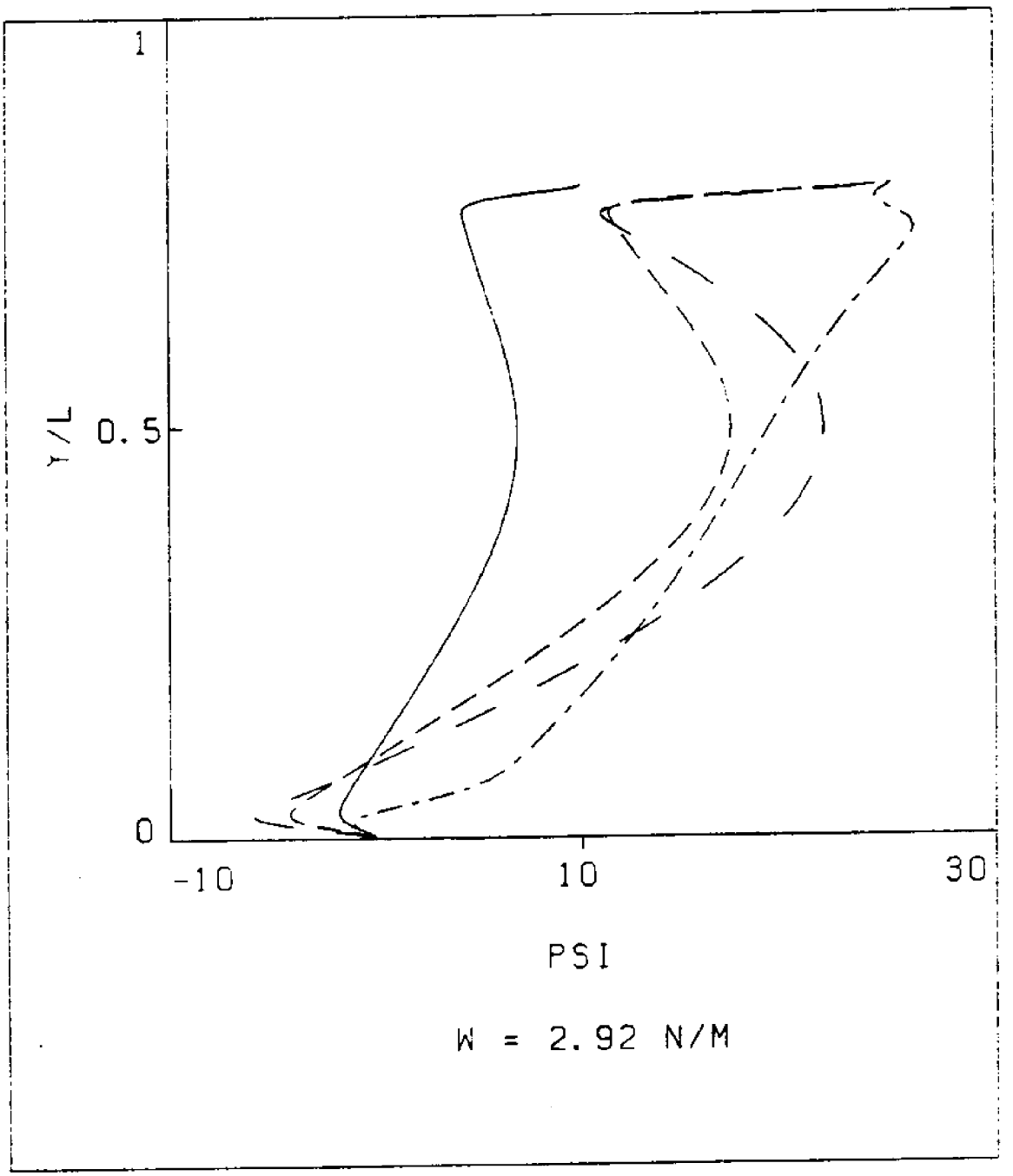

Figure 4-11: ψ_0 Versus y_0 For Case 1 And Four 3-D Excitation Conditions

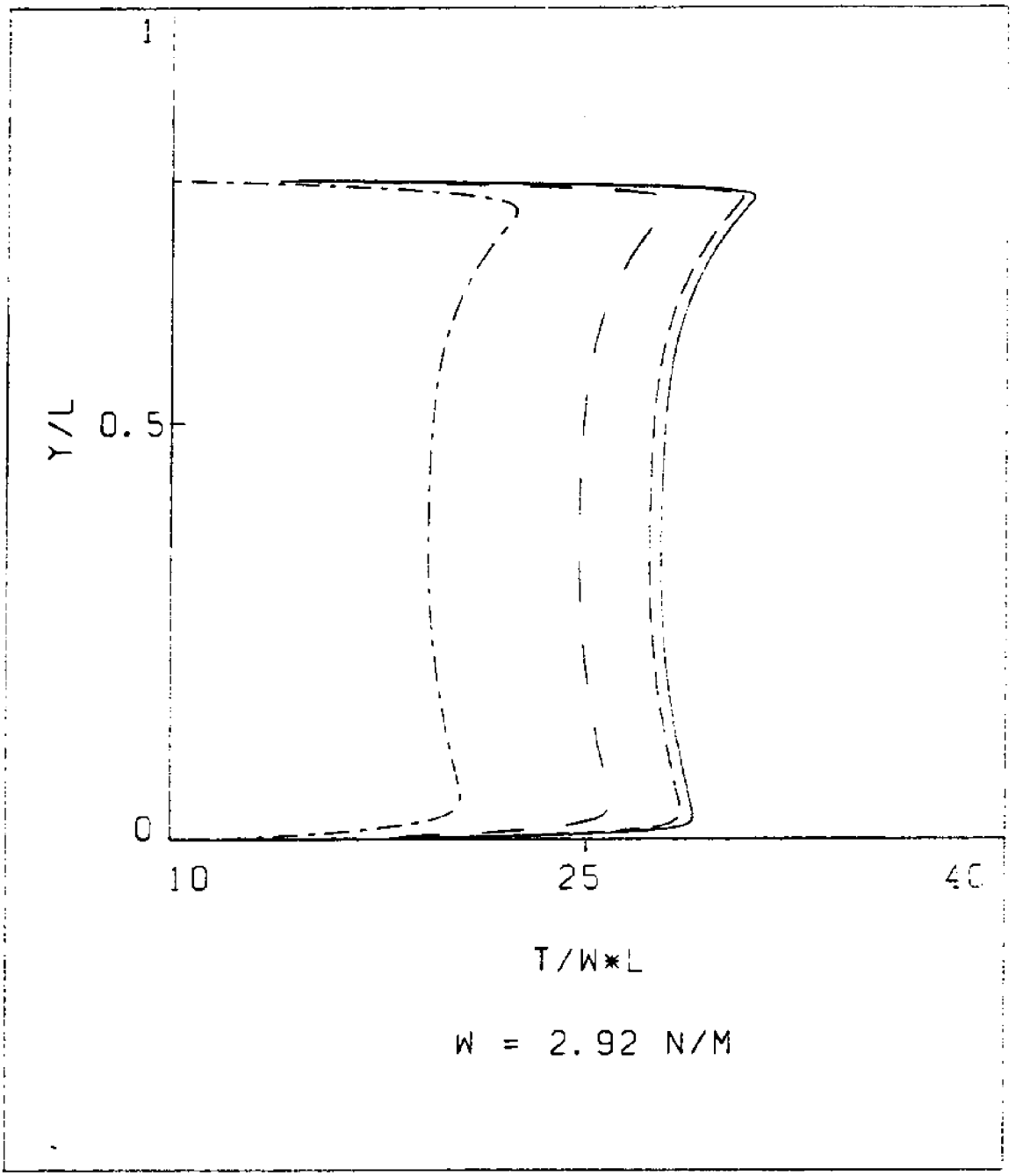

Figure 4-12: T_0 Versus y_0 For Case 1 And Four 3-D Excitation Conditions

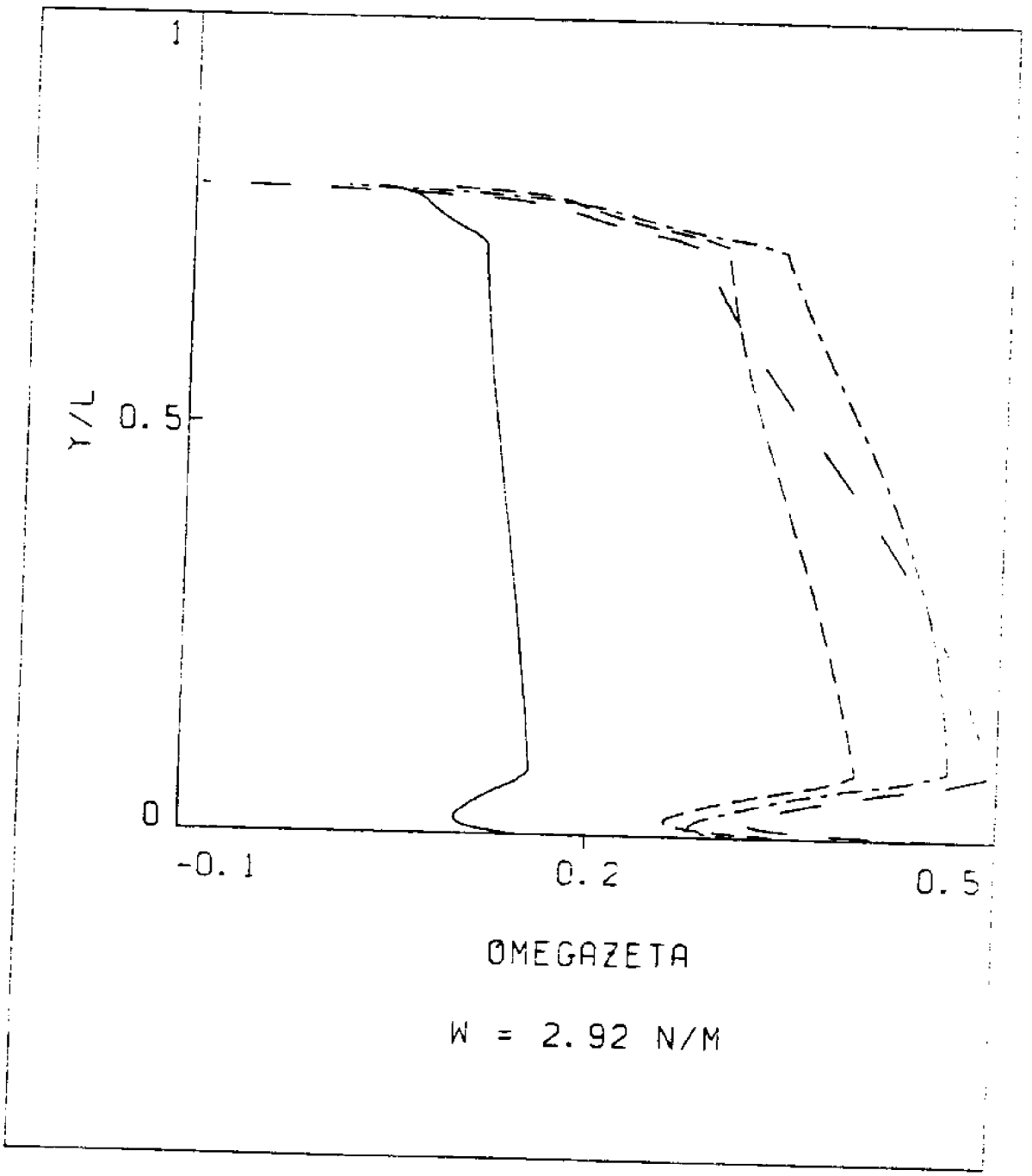

Figure 4-13: Ω_0^{ζ} Versus y_0 For Case 1 And Four 3-D Excitation Conditions

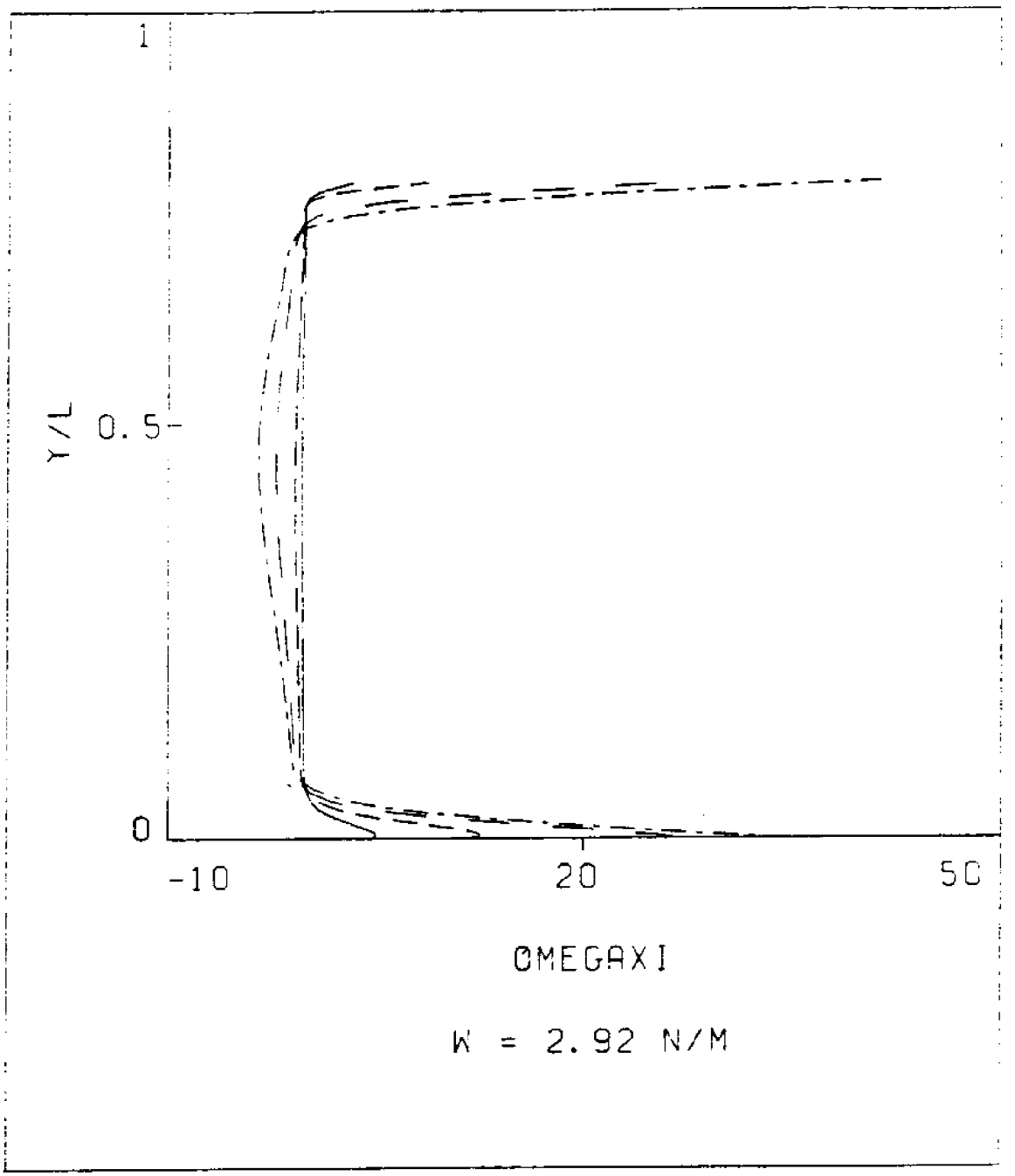

Figure 4-14: Ω_o^{ξ} Versus y_o For Case 1 And Four 3-D Excitation Conditions

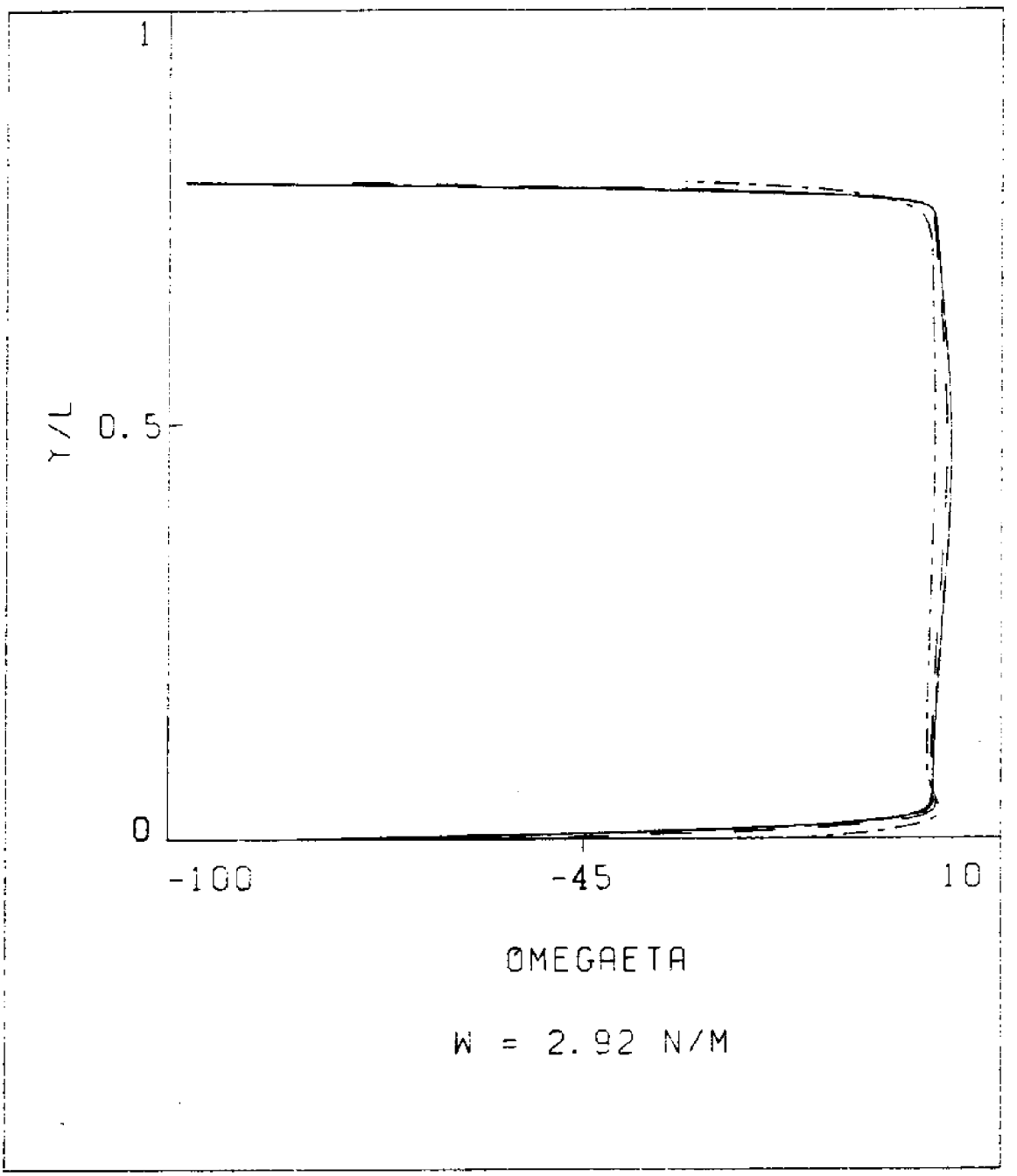

Figure 4-15: Ω_0^{η} Versus y_0 For Case 1 And Four 3-D Excitation Conditions

Coming now to Case 2, where the top end of the riser has an offset of x_T=6.10 m and, due to increase of water level, y_T=82.30 m. Here, again the riser is subject to a linear strong current in the x direction with $V_x(0)$=1.03 m/s and $V_x(h_w)$=1.55 m/s where $h_w=h_i$=85.34 m. In addition, $\psi_0(L)$=0 and, therefore, the riser has a two-dimensional configuration in the XY plane without torsion. Figures 4-16 and 4-17 show the results for this excitation condition, obtained be executing our two-dimensional static program. The initial approximation for our embedding technique was obtained using the method of Section 3.2 for a constant current equal to 1.29 m/s, the mean value of the actual currect. As in Case 1, Condition 1, our procedure slowly applies the effective weight forces and modifies the current to the actual linear profile. Figure 4-16 shows the displacement x_0 (solid line) and the angle ϕ_0 (dashed line) as a function of y_0. Figure 4-17 shows the component of the rate of rotation Ω_0^η (solid line) and the effective tension T_0 (dashed line) as a function of y_0. Again, all variables plotted are non-dimensional.

The comments pertaining to the response for Case 1, Condition 1 also hold in the present excitation condition. The maximum effective tension for Case 2 is equal to 16.6 kN and the maximum tension is 55.6 kN. The tension due to internal overpressure again amounts to 39.8 kN. The increase of the effective tension with respect to Case 1, Condition 1 is a result of a decreased sag due to the change of the position of the top end with respect to the lower end of the

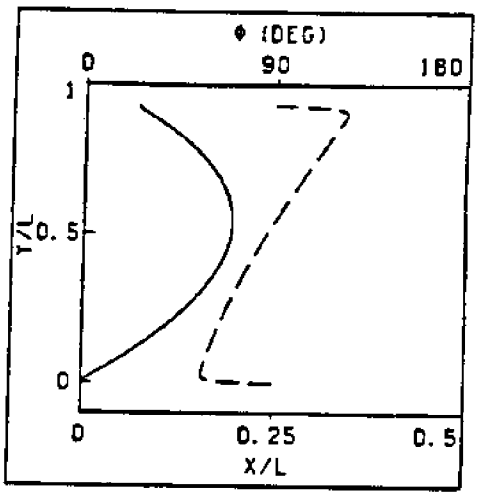

Figure 4-16: x_o And ϕ_o Versus y_o For Case 2

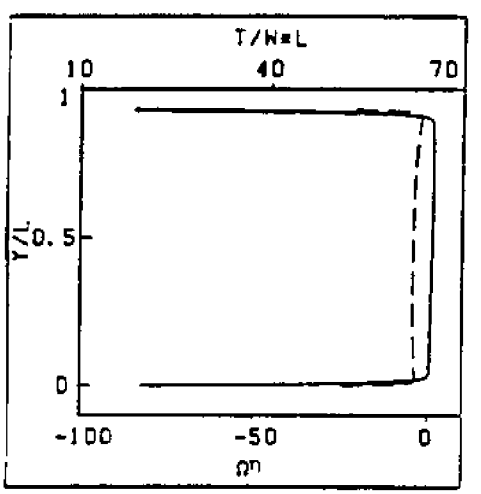

Figure 4-17: Ω_o^{η} And T_o Versus y_o For Case 2

riser. Finally, the minimum bending radius for the present case is 1.05 m, i.e. 16.4% larger than the corresponding value for Case 1, Condition 1 and therefore less critical. As stated before, the value of the minimum bending radius is an important design parameter and needs to be controlled with appropriate strain relief units at the ends.

Chapter 5

NUMERICAL RESULTS FOR A BUOYANT RISER WITH A SINGLE BUOYANCY MODULE

The riser analyzed in this Section is made up of two flexible tubes with inner diameter of 85.7 mm and outer diameter of 122.9 mm clamped together and having the same structural characteristics as in Chapter 4. However, this riser does not have small uniformly distributed buoyancy modules as the riser of Chapter 4. The present riser is supported by a single large buoyancy module placed at approximately 1/3 of the length from the lower end, which gives the configuration a lazy S shape. This example was selected because no numerical data for lazy S configurations was available to us and only in order to test our computer program for a situation involving sharp changes of the structural characteristics of the riser such as those occurring in the presence of large buoyancy module or buoy at some point along the length of the riser.

The overall riser characteristics are: L=88.392 m; W_a=125.55 N/m; EA=267 MN; A_o=237.4 cm^2; A_i=115.4 cm^2; ρ_i=820 kg/m^3; p=3.45 MPa; c=0; vertical distance of lower support, s=0, from ocean floor is 7.62 m.

For the bare riser sections, we used the following additional characteristics: $W=251.1$ N/m; $EI^{\eta\eta}=3.3$ kN.m^2; $EI^{\xi\xi}=12.2$ kN.m^2; $GI^{p}=0.582$ MN.m^2; $D^{\xi}=0.2458$ m; $D^{\eta}=0.1229$ m; $P_e^{\xi\eta}=0.772$ m; $m=49.93$ kg/m, $m^{\zeta}=40.47$ kg/m; $m_a^{\zeta}=0$; $m_a^{\xi}=48.638$ kg/m; $m_a^{\eta}=12.16$ kg/m; $J^{\zeta\zeta}=0.4932$ kg.m, $J_a^{\zeta\zeta}=0.0781$ kg.m. The bare riser sections extend for $l_1=28.964$ m and $l_2=57.928$ m from s=0 and s=L, respectively.

For the riser sections covered by the buoyancy module we used: $W=-7147.4$ N/m; $EI^{\eta\eta}=89.1$ MN.m^2; $EI^{\xi\xi}=89.1$ MN.m^2; $GI^{p}=69.1$ MN.m^2; $D^{\xi}=D^{\eta}=1.269$ m, $P_e^{\xi\eta}=20.53$ m; $m=566.4$ kg/m; $m^{\zeta}=556.9$ kg/m; $m_a^{\zeta}=1271.4$ kg/m; $m_a^{\xi}=m_a^{\eta}=1296.4$ kg/m; $J^{\zeta\zeta}=106.51$ kg.m; $J_a^{\zeta\zeta}=0$. In order to model the transition of the structural rigidities between the bare riser sections and those covered by the buoyancy module, we assumed that the bare riser rigidities increased linearly to the above rigidities within 0.2 m from each end of the buoyancy module. The physical length of the buoyancy module is $L_b=1.5$ m so that $L=l_1+L_b+l_2$. The lower end of the buoyancy module is at $s=l_1$ from the lower end.

In this work we studied two two-dimensional excitation conditions at a water depth of 72.62 m with $h_w=h_i=65$ m, $x_T=20$ m and $y_T=62$ m in the presence of unidirectional strong currents. In the first case we used a constant current with $V_x=2$ m/s and the second case a linear current with $V_x(0)=1.03$ m/s and $V_x(h_w)=1.55$ m/s. Given that the average effective weight per unit length $W_a=125.55$ N/m is now significant as compared to the current force due to the mean value of the

current, $0.5\rho_w C_D \bar{D}^{\xi} \bar{V}_x |\bar{V}_x|$ where $\bar{D}^{\xi}$=0.263 m is the mean diameter, we started the embedding procedure using as initial current a very strong constant current with V_x=5 m/s for which the initial analytical approximation of Section 3.2 is expected to be reasonable and solved the problem for V_x=5 m/s accurately including all forces. Using this converged solution for V =5 m/s as initial approximation, we solved the problem for a constant current V_x=3.5 m/s using our embedding technique. This last solution was subsequently used as initial approximation for the solution of a static problem for a constant current V_x=2.75 m/s determined using our embedding technique. Finally, this solution for V_x=2.75 m/s was used as initial approximation of our first static problem involving a constant current with speed V_x=2 m/s. The solution for V_x=2 m/s was used as initial approximation for the solution of our second static excitation case involving a linear current. In order to accurately resolve the structural changes at the ends of the buoyancy module, a sufficiently large number of initial points need to be used to start the process correctly. So, for example, our initial analytical solution for V_x=5 m/s used 120 uniformly distributed points, which provides three discretization points within the buoyancy module. Our final solution for the constant and linear currents involves 18 discretization points within the buoyancy module out of a total of 195 dicretization points. The remaining 57 discretization points beyond the 120 original points are densely distributed close to s=0, s=L, $s=l_1$, $s=l_1+L_b$ to

provide accurate resolution of regions involving sharp changes of the solution. The addition of new discretization points beyond the original 120 is done automatically by the program in order to reduce and equidistribute the error on the final mesh [18].

Figures 5-1 to 5-3 and 5-4 to 5-6 show our results for the constant 2 m/s current and the linear current respectively. Figures 5-1 and 5-4 show the displacement x_0 (solid line) and the angle ϕ_0 in degrees (dashed line) as a function of y_0. Subscript o denoting static quantities was dropped for convenience in the figures. Figures 5-2 and 5-5 show the rate of rotation Ω_0^η (solid line) and the effective tension T_0 (dashed line) as a function of y_0. Figures 5-3 and 5-6 show the shear force Q_0^ξ (solid line) and the tension in the material P_0 (dashed line) as a function of y_0. All variables plotted except ϕ_0 are non-dimensional. Lengths are non-dimensionalized by L and forces by $W_a L \approx 11.1$ kN.

For the case of constant current 2 m/s, the buoyancy module lies approximately between $y_0 = 0.1809$ and 0.1854 and for the case of the linear current between $y_0 = 0.2367$ and 0.2284. In terms of arc length the buoyancy module lies approximately between s=0.3277 and 0.3447. The plots of ϕ_0, Ω_0^η, T_0, Q_0^ξ and P_0 indicate a very sharp change of the solution near the ends and near the position of the buoyancy module, as expected. For the constant current case the minimum bending radius occurs at s=0 and is approximately equal to 0.406 m, while for the weaker linear current case, this occurs near the buoyancy

module and is equal to 0.440 m. This occurs because the relative importance of the buoyancy force from the module as compared to the normal drag force increased from the first to the second excitation case. The above values of the bending radii are excessively small which indicates that improvements in the design of the system should be made. This was not attempted because the present system and excitation were only chosen to exhibit the applicability of our program for very non-uniform systems. We expect however that strain relief units at the ends and the connection with buoys and more uniformly distributed modules will provide the tools to achieve better performance.

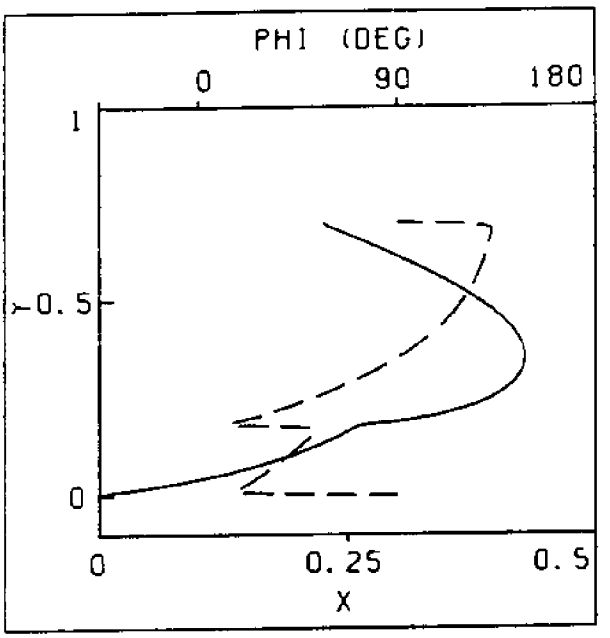

Figure 5-1: x_0 And ϕ_0 Versus y_0
For Constant Current 2 m/s

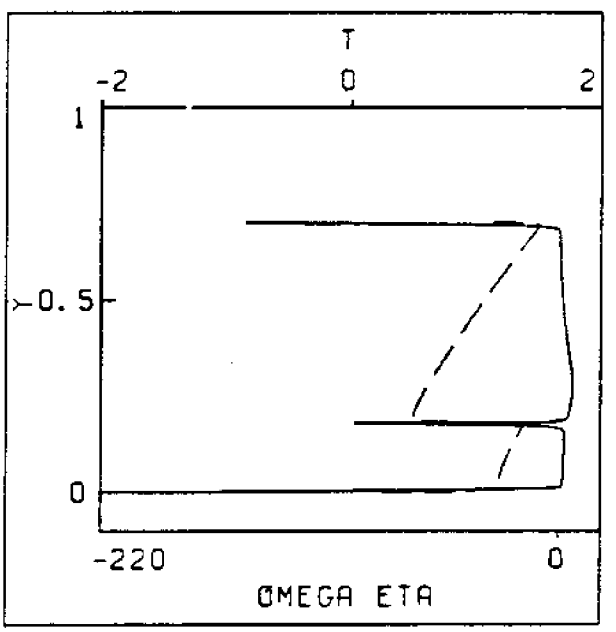

Figure 5-2: Ω_0^n And T_0 Versus y_0
For Constant Current 2 m/s

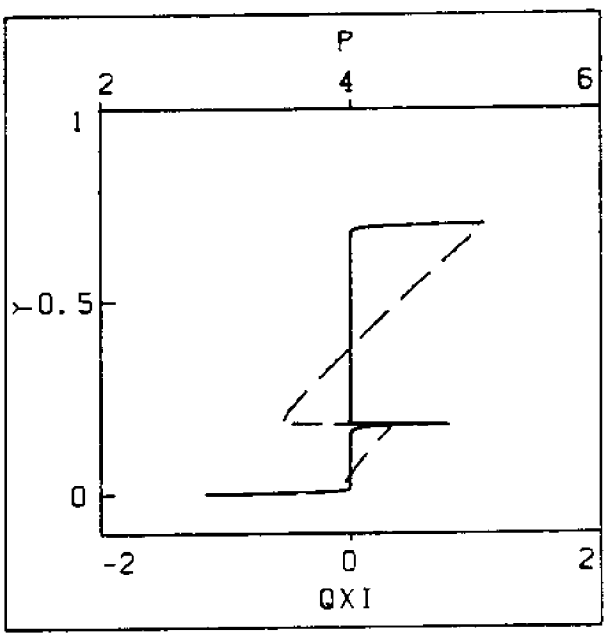

Figure 5-3: Q_0^{ξ} And P_0 Versus y_0 For Constant Current 2 m/s

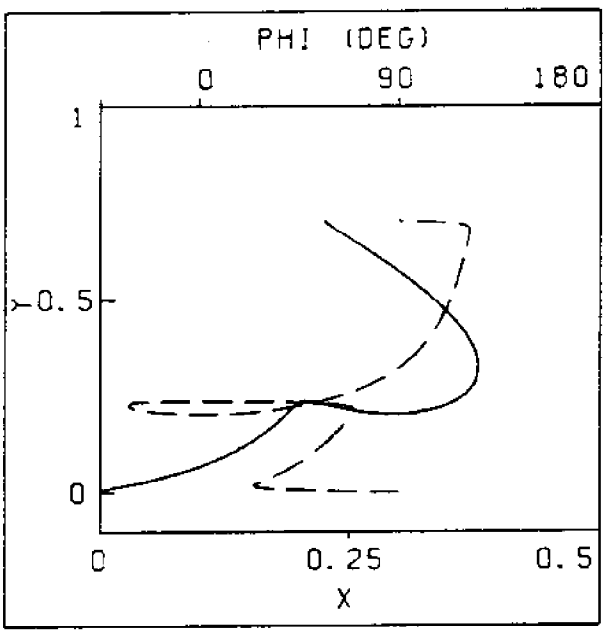

Figure 5-4: x_o And ϕ_o Versus y_o For A Linear Current

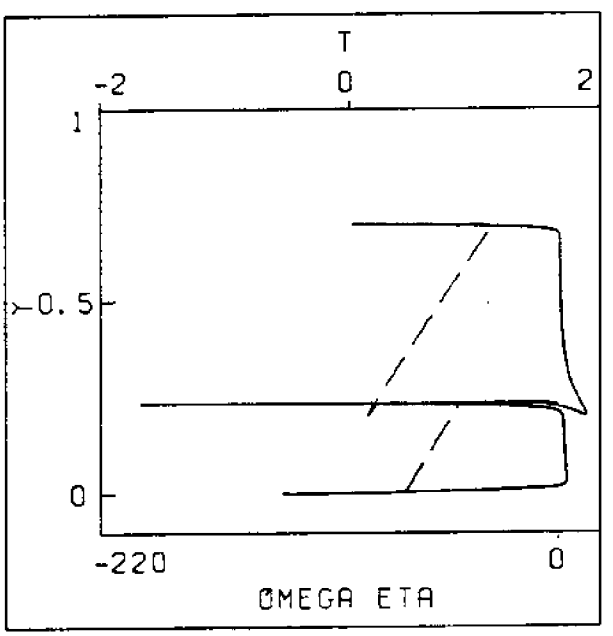

Figure 5-5: Ω_o^η And T_o Versus y_o For A Linear Current

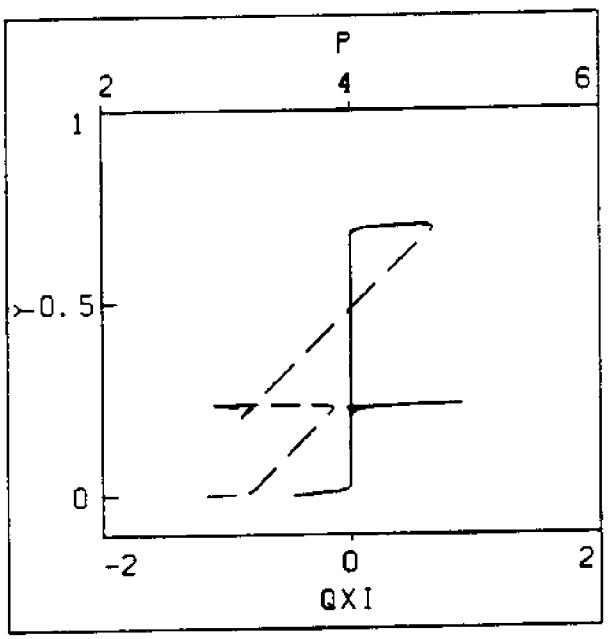

Figure 5-6: Q_o^{ξ} And P_o Versus y_o For A Linear Current

REFERENCES

1. Love, A.E.H., A Treatise on the Mathematical Theory of Elasticity. 4th ed. Mineola, NY: Dover, 1944.

2. Landau, L.D. and Lifshitz, E. M., Theory of Elasticity. Elmsford, NY: Pergamon, 1970.

3. Nordgren, R.P., "Dynamic Analysis of Marine Risers With Vortex Excitation"., Journal of Energy Resources Technology, ASME Trans. 104 (1982) 14-19.

4. Patrikalakis, N.M., Theoretical and Experimental Procedures For the Prediction of the Dynamic Behavior of Marine Risers. Ph.D. Thesis, Cambridge, Mass.: M.I.T. Dept. of Ocean Engineering, 1983.

5. Nordgren, R.P. "On the Computation of the Motion of Elastic Rods". Journal of Applied Mechanics, 96 (1974) 777-780.

6. Garrett, D.L., "Dynamic Analysis of Slender Rods" Journal of Energy Resources Technology, ASME Trans 104 (1982) 302-306.

7. Patrikalakis, N.M. and Chryssostomidis, C., A Mathematical Model For Compliant Risers. Cambridge, Mass.: M.I.T. Sea Grant Report 85-17, 1985.

8. Patrikalakis, N.M. and Chryssostomidis, C., "Vortex Induced Response of a Flexible Cylinder in a Constant Current". Journal of Energy Resources Technology, ASME Trans 107 (1985) 244-249.

9. Patrikalakis, N.M. and Chryssostomidis, C., "Vortex Induced Response of a Flexible Cylinder in a Sheared Current". Proceedings of the 4th International Symposium on Offshore Mechanics and Arctic Engineering, Dallas, Texas, 1985. vI, pp. 593-600. NY: ASME, 1985.

10. Crandall, S.H. et al, Dynamics of Mechanical and Electromechanical Systems. NY: McGraw Hill, 1968.

11. de Oliveira, J.G. and Morton, A.W., "Floating Production Systems With Vertical Flexible Risers". Proceedings of the Indonesian Petroleum Association 13th Annual Convention, 1984. Djakarta, Indonesia: IPA, 1984.

12. de Oliveira, J.G., Goto, Y. and Okamoto, T., "Theoretical and Methodological Approaches to Flexible Pipe Design and Application". Proceedings of the 17th Offshore Technology Conference, 1985. v3, Paper OTC 5021, pp. 517-526. Houston, Texas: OTC, 1985.

13. Panicker, N.N. and Yancey, I.R., "Deepwater Production Riser". Proceedings of the 15th Offshore Technology Conference, 1983. v2, Paper OTC 4512, pp. 9-18. Houston, Texas: OTC, 1983.

14. Sarpkaya, T. and Isaacson, M., Mechanics of Wave Forces on Offshore Structures. NY: Van Nostrand, 1981.

15. Newman, J.N., Marine Hydrodynamics. Cambridge, Mass.: M.I.T. Press, 1977.

16. Keller, H.B., Numerical Methods For Two-Point Boundary Value Problems. Waltham, Mass.: Blaisdell, 1968.

17. Ferziger, J.H., Numerical Methods For Engineering Application. NY: Wiley, 1981.

18. Pereyra, V. "PASVA3: An Adaptive Finite Difference Fortran Program For First Order Nonlinear Ordinary Boundary Problems". Codes For Boundary Value Problems in Ordinary Differential Equations. Edited by B. Child, et al. Lecture Notes in Computer Science, v76, pp. 67-88. NY: Springer, 1979.

19. Chryssostomidis, C. and Patrikalakis, N.M., "Compliant Riser Analysis". Proceedings of the International Symposium on Ocean Space Utilization, Tokyo, Japan, 1985. v1, pp. 401-410. NY: Springer, 1985.

20. NAG, Numerical Algorithms Group FORTRAN Library. Oxford, England: NAG, 1985.

21. Carrier, G.F. and Pearson, C.E., Ordinary Differential Equations. Waltham, Mass.: Blaisdell, 1968.

22. Powell, M.J.D., "A Hybrid Method For Nonlinear Albegraic Equations". Numerical Methods For Nonlinear Algebraic Equations. Edited by P. Rabinowitz. pp. 87-161. NY: Gordon and Breach, 1970.

Table of Contents

List of Figures